


Author: P.C. Broekema	Date of issue: 2004-May-16 Kind of issue: Limited	Scope: Project documentation Doc.nr.: LOFAR-ASTRON-MEM-136	
	Status: For Review Revision nr.: 1.0	File: <a href="http://dop47.nfra.nl/chris/Thesis/Thesis.pdf">http://dop47.nfra.nl/chris/Thesis/Thesis.pdf</a>	

## Numerical analysis of the LOFAR remote station beamformer

P.C. Broekema




Verified:			
Name	Signature	Date	Rev.nr.
M. van Veelen	.....	.....	.....

Accepted:		
Work Package Manager	System Engineering Manager	Program Manager
M. van Veelen	C.M. de Vos	J. Reitsma
.....	.....	.....
<i>date:</i>	<i>date:</i>	<i>date:</i>

©ASTRON 2004

All rights are reserved. Reproduction in whole or in part is prohibited without the written consent of the copyright owner.


Author: P.C. Broekema	Date of issue: 2004-May-16 Kind of issue: Limited	Scope: Project documentation Doc.nr.: LOFAR-ASTRON-MEM-136	
	Status: For Review Revision nr.: 1.0	File: <a href="http://dop47.nfra.nl/chris/Thesis/Thesis.pdf">http://dop47.nfra.nl/chris/Thesis/Thesis.pdf</a>	

## Distribution list:

Group:	For Information:
ASTRON                      RuG M. van Veelen              R. Moddemeijer J. Dromer                      S. Achterop S.J. Wijnholds	

## Document revision:


Revision	Date	Section	Page(s)	Modification
0.5	2003-Jul-30	-	-	Creation
0.6	2003-Nov-05	-	-	Version for initial review
0.7	2003-Nov-20	-	-	Revised structure according to review comments
0.9	2003-Dec-16	-	-	Second review comments incorporated
0.99	2004-Jan-12	-	-	First version for review at RuG
1.0	2004-May-16	-	-	Final version

Author: P.C. Broekema	Date of issue: 2004-May-16 Kind of issue: Limited	Scope: Project documentation Doc.nr.: LOFAR-ASTRON-MEM-136	
	Status: For Review Revision nr.: 1.0	File: <a href="http://dop47.nfra.nl/chris/Thesis/Thesis.pdf">http://dop47.nfra.nl/chris/Thesis/Thesis.pdf</a>	

### Abstract


LOFAR (LOw Frequency ARray) is a large new radio telescope aimed at unusually low frequencies under development at ASTRON. Using phased array technology, one of the instrumental components of this system is the beamformer using phase shifters. The use of phase shifters over physical time delay devices reduces cost of the system and increases flexibility. Phase shifters allow us to create multiple beams at hardly any extra cost and it opens the possibility of adaptive responses to interfering signals.

The unusual frequencies, combined with the desire to use non regular array configurations for the system means that analytical analysis of the station beamformer is hard, if not impossible. We therefore introduce a numerical analysis of the station beamformer using simulations of the LOFAR station both in Matlab and in C++.


Author: P.C. Broekema	Date of issue: 2004-May-16 Kind of issue: Limited	Scope: Project documentation Doc.nr.: LOFAR-ASTRON-MEM-136	
	Status: For Review Revision nr.: 1.0	File: <a href="http://dop47.nfra.nl/chris/Thesis/Thesis.pdf">http://dop47.nfra.nl/chris/Thesis/Thesis.pdf</a>	

## Contents


<b>1</b>	<b>Introduction</b>	<b>8</b>
1.1	A short history of radio astronomy . . . . .	8
1.2	Optimizing cost and quality . . . . .	10
1.3	Current status of the LOFAR project . . . . .	10
1.4	Problem statement . . . . .	11
1.5	Constraints . . . . .	11
1.5.1	Astronomers . . . . .	11
1.5.2	Calibration . . . . .	11
1.5.3	Radio Frequency Interference (RFI) . . . . .	12
<b>2</b>	<b>Background information</b>	<b>13</b>
2.1	Coordinate systems . . . . .	13
2.2	Introduction of basic concepts . . . . .	14
2.2.1	Sensitivity . . . . .	14
2.2.2	Resolution . . . . .	14
2.2.3	Beamforming and delay compensation . . . . .	15
2.2.4	Adaptive beamforming . . . . .	15
2.2.5	Beam shape . . . . .	17
2.2.6	Side lobes . . . . .	19
2.2.7	Grating lobes - regular arrays . . . . .	19
2.2.8	Grating lobes - irregular arrays . . . . .	19

Author: P.C. Broekema	Date of issue: 2004-May-16 Kind of issue: Limited	Scope: Project documentation Doc.nr.: LOFAR-ASTRON-MEM-136	
	Status: For Review Revision nr.: 1.0	File: <a href="http://dop47.nfra.nl/chris/Thesis/Thesis.pdf">http://dop47.nfra.nl/chris/Thesis/Thesis.pdf</a>	


2.2.9	Beam squint . . . . .	20
2.3	Interference subspace estimation and spatial projection . . . . .	20
2.3.1	Minimum variance . . . . .	22
2.3.2	Estimating the Interference subspace . . . . .	23
2.3.3	Subspace Tracking . . . . .	23
<b>3</b>	<b>Array Processing techniques</b>	<b>24</b>
3.1	Deterministic suppression . . . . .	24
3.2	Automatic detection techniques . . . . .	25
3.2.1	Eigen value based techniques . . . . .	25
3.2.2	Projection Approximation Subspace Tracking with deflation . . . . .	25
3.3	Determine the number of sources . . . . .	27
3.3.1	Thresholding . . . . .	27
3.3.2	Minimum Description Length (MDL) . . . . .	27
3.4	RFI suppression techniques . . . . .	27
3.4.1	Spatial Projection . . . . .	27
<b>4</b>	<b>Development of simulation environment</b>	<b>30</b>
4.1	Simulation environment . . . . .	30
4.1.1	Matlab - StationGUI . . . . .	30
4.1.2	C++ StationSim . . . . .	30
4.1.3	Data generators . . . . .	31
4.1.4	Limitations of current simulations . . . . .	32

Author: P.C. Broekema	Date of issue: 2004-May-16 Kind of issue: Limited	Scope: Project documentation Doc.nr.: LOFAR-ASTRON-MEM-136	
	Status: For Review Revision nr.: 1.0	File: <a href="http://dop47.nfra.nl/chris/Thesis/Thesis.pdf">http://dop47.nfra.nl/chris/Thesis/Thesis.pdf</a>	

<b>5</b>	<b>Numerical analysis of the station beamformer</b>	<b>33</b>
5.1	Nulling impact . . . . .	33
5.1.1	Introduction . . . . .	33
5.1.2	Experiment description . . . . .	33
5.1.3	Quality measures . . . . .	34
5.1.4	Experimental results . . . . .	35
5.1.5	Halfpower beamwidth . . . . .	35
5.1.6	Maximum sidelobe level . . . . .	37
5.1.7	Conclusions and recommendations . . . . .	38
5.2	Beam squint . . . . .	39
5.2.1	Introduction . . . . .	39
5.2.2	Experiment description . . . . .	39
5.2.3	Quality measures . . . . .	40
5.2.4	Theoretical expectations . . . . .	40
5.2.5	Experimental results . . . . .	41
5.2.6	Conclusions and recommendations . . . . .	42
5.3	Technique evaluation (EVD, SVD, PASTd) . . . . .	42
<b>6</b>	<b>Conclusions and recommendations</b>	<b>45</b>
6.1	Baseline design . . . . .	45
6.2	Limitations . . . . .	46
6.3	Recommendations . . . . .	47

Author: P.C. Broekema	Date of issue: 2004-May-16 Kind of issue: Limited	Scope: Project documentation Doc.nr.: LOFAR-ASTRON-MEM-136	
	Status: For Review Revision nr.: 1.0	File: <a href="http://dop47.nfra.nl/chris/Thesis/Thesis.pdf">http://dop47.nfra.nl/chris/Thesis/Thesis.pdf</a>	

<b>7</b>	<b>Final words</b>	<b>48</b>
7.1	Personal review . . . . .	48
7.2	Acknowledgments . . . . .	48
<b>A</b>	<b>Fitting of a second order paraboloid</b>	<b>52</b>
<b>B</b>	<b>Scanning the sky</b>	<b>54</b>
<b>C</b>	<b>Solving a set of equations</b>	<b>55</b>

Author: P.C. Broekema	Date of issue: 2004-May-16 Kind of issue: Limited	Scope: Project documentation Doc.nr.: LOFAR-ASTRON-MEM-136	
	Status: For Review Revision nr.: 1.0	File: <a href="http://dop47.nfra.nl/chris/Thesis/Thesis.pdf">http://dop47.nfra.nl/chris/Thesis/Thesis.pdf</a>	

# 1 Introduction

## 1.1 A short history of radio astronomy

Modern radio astronomy started in the 1930's at relatively low frequencies. The first radio observations were made in 1932 by Karl Jansky, an engineer of the Bell Telephone Laboratories in Holmdel, NJ. Bell Labs wanted to investigate using "short waves" (wavelengths of about 10-20 meters) for transatlantic radio telephone service. Jansky was assigned the job of investigating the sources of static that might interfere with radio voice transmissions.

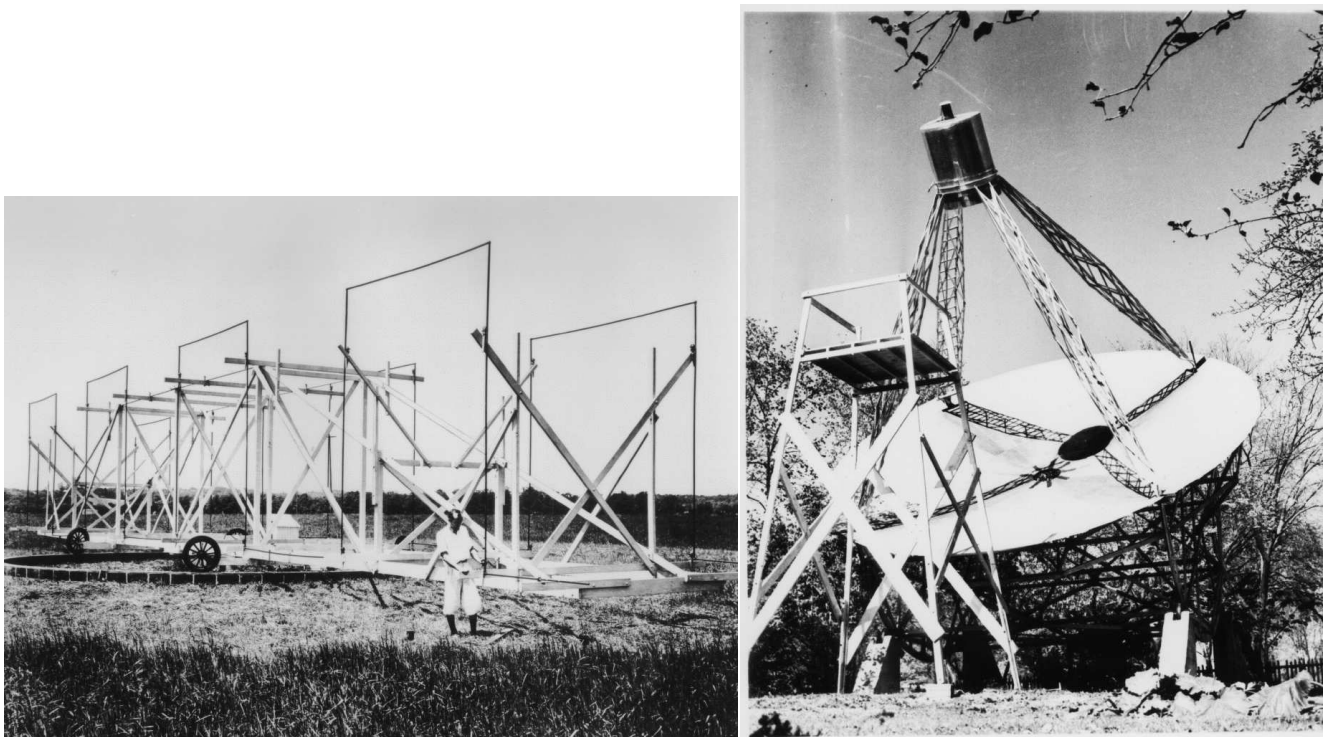



Figure 1: Jansky's rotating antenna ca. 1932 and Reber's telescope ca. 1938

He built an antenna, as seen on the left in figure 1, designed to receive radio waves at a frequency of 20.5 MHz (wavelength about 14.5 meters). It was mounted on a turntable that allowed it to rotate in any direction, earning it the name "Jansky's merry-go-round". By rotating the antenna, one could find what the direction was to any radio signal. This eventually resulted in the discovery of a strong source of radio static originating from the central region of our galaxy, the Milky Way. Many scientists were fascinated by Jansky's discovery, but the great depression prevented anyone from following up on it for several years.

Only a young engineer named Grote Reber, using his own funds, constructed a 31.4 foot (about 9.5 meter) diameter dish in his back yard (on the right in figure 1). His first receiver, designed for 3300 MHz



Author: P.C. Broekema	Date of issue: 2004-May-16 Kind of issue: Limited	Scope: Project documentation Doc.nr.: LOFAR-ASTRON-MEM-136	
	Status: For Review Revision nr.: 1.0	File: <a href="http://dop47.nfra.nl/chris/Thesis/Thesis.pdf">http://dop47.nfra.nl/chris/Thesis/Thesis.pdf</a>	

failed to detect signals from outer space. So did the second, at 900 MHz. Finally a third receiver at 160 MHz (1.9 meters wavelength) was successful in detecting radio emission from the Milky Way, in 1938, confirming Jansky's discovery.

Despite the fact that these early pioneers did research at relatively low frequencies, most later radio astronomy has been concentrated on higher frequencies. The first detection of the spectral line emissions of neutral hydrogen at rest (at 1420.40575 MHz), the most prolific element in our universe, was certainly an important reason for this shift in attention, but the fact that these higher frequencies penetrate the earth's ionosphere with more ease was also a factor.

This does not mean that these lower frequency bands hold no interesting information. Quite the contrary in fact. The universe is expanding, it has since it's creation. Looking at objects further away means looking back in time, since emissions from these objects take such a long time to get here. These objects, having traveled this great distance in the lifetime of the universe, must have traveled faster than objects closer by. The Doppler shift this introduces, might place these very old objects in a much lower frequency range than current radio telescopes can observe.

Recent advances in available computing power and data processing algorithms should enable us to observe at these lower frequencies despite the limitations. Ionospheric correction is currently sufficient to correct for the signal distortions introduced by the Earth's outer atmosphere. Building on experience with antenna arrays like the Westerbork Synthesis Radio Telescope (WSRT) and, more recently, by using several of these antenna arrays together on a continental scale, a process called VLBI (Very Long Baseline Interferometry), a radio telescope of an entirely new generation has been designed. This telescope will be called LOFAR, which stands for LOw Frequency ARray, and will observe frequencies ranging from 10 to 250 MHz.

The problems associated with these lower frequencies are numerous. The atmospheric distortions are already mentioned. The lower frequency, and therefore longer wavelength, means that the diameter telescope needs to be larger than with higher frequencies, to attain sufficient resolution. By using digital data processing techniques and glass-fiber to interconnect a large number of antenna fields, we are able to create a telescope of the scale that is required to provide sufficient resolution at the frequencies specified.

LOFAR will consist of a large number of small wideband antennas (approximately 25.000). These antennas are placed in about a hundred fields, each about the surface of a football field. Stations will be connected by glass-fiber to a central core, providing the bandwidth needed to transmit the tremendous amount of data generated by the array. An impression of the layout of the LOFAR array is given in figure 2. It also shows the scale of the array. To achieve the desired resolution at this frequency, an array with a diameter of about three hundred and fifty kilometers is needed.


Author: P.C. Broekema	Date of issue: 2004-May-16 Kind of issue: Limited	Scope: Project documentation Doc.nr.: LOFAR-ASTRON-MEM-136	
	Status: For Review Revision nr.: 1.0	File: <a href="http://dop47.nfra.nl/chris/Thesis/Thesis.pdf">http://dop47.nfra.nl/chris/Thesis/Thesis.pdf</a>	



Figure 2: Possible LOFAR configuration projected on the Netherlands and Germany

## 1.2 Optimizing cost and quality


Looking at figure 2 it becomes obvious that a conventional dish antenna of this scale is not practical. The challenge now is to design a practical telescope that is also affordable. In LOFAR, the choice was made to maximize the performance of the telescope for a fixed budget.

Reducing the complexity of the individual array elements is an effective way to maximize the collecting area. By making the antennas static and thus removing the equipment needed to point the antennas in a specific direction, we can drastically reduce element cost. This is not a new idea, modern radar systems use phased arrays which are based on the same principle.

Two added advantages of using a beamformer are the significant reduction in data it produces and the fact that we can use the beamformer to spatially filter out interfering signals.

## 1.3 Current status of the LOFAR project

Recently the preliminary design of the LOFAR array has been approved. The first prototype station (ITS - Initial Test Station) is under construction near Exloo as I write this, and a small test array called THETA (Ten Heterogeneous Element Test Array) has been operational since September 2003. The aim of these prototypes is to validate the functional design of the antennas, receiver units and signal processing

Author: P.C. Broekema	Date of issue: 2004-May-16 Kind of issue: Limited	Scope: Project documentation Doc.nr.: LOFAR-ASTRON-MEM-136	
	Status: For Review Revision nr.: 1.0	File: <a href="http://dop47.nfra.nl/chris/Thesis/Thesis.pdf">http://dop47.nfra.nl/chris/Thesis/Thesis.pdf</a>	

algorithms. Real-time processing, a requirement for the eventual LOFAR stations, will not be done at this point.

## 1.4 Problem statement

Since the individual array elements cannot move, we need another way to point the array to a specific point on the sky. This is done using a so called beamformer. By introducing specific time delays per antenna, the total array can be aimed to where we want it to. Beamforming is however a technique that is normally done on quite narrow frequency bands and the theory specifically mentions that beamforming on larger frequency bands might cause problems.

So we need to examine the effects wider band signals have on the LOFAR beamformer. Ideally we would like to have an approximate value for the maximum bandwidth we can safely beamform with the LOFAR beamformer.

The beamformer could be used to spatially filter out interfering signals. This would however affect the output signal in some way. We need to know in what way spatial filtering will distort the signal.

## 1.5 Constraints


### 1.5.1 Astronomers

The astronomers are of course our main clients. Everything the remote station beamformer does to the signal is in some way connected to requirements made by the astronomical community. The main requirement from the astronomical community is a stable and clean signal from the LOFAR station. This is a direct consequence of the fact that astronomical signals are so weak, that we need to integrate over a large number of samples in order to observe anything. Any processing we do on the signal therefore needs to preserve the beampattern within at least the  $-3dB$  top. Any abrupt changes in output power need to be avoided.

It must be mentioned that the requirements from the astronomical corner are not at all stable and subject to change. The requirements mentioned here are broad guidelines on which we can build a system. More detailed requirements are, of course, available in the various design documents[1][13][15].

### 1.5.2 Calibration

One of the first tasks to be performed once a LOFAR station has been placed in the field, is to calibrate the antennas. Using a holographic scanning technique using two beams, one pointing at a known source

Author: P.C. Broekema	Date of issue: 2004-May-16 Kind of issue: Limited	Scope: Project documentation Doc.nr.: LOFAR-ASTRON-MEM-136	
	Status: For Review Revision nr.: 1.0	File: <a href="http://dop47.nfra.nl/chris/Thesis/Thesis.pdf">http://dop47.nfra.nl/chris/Thesis/Thesis.pdf</a>	

and one scanning over the sky, small gain and phase deviations are detected and canceled.

This calibration technique requires that the signal is totally clean of any disturbances. This means that any frequency band about to be used to calibrate the station, is first examined for interfering signals. If interferers are detected, this frequency band is discarded and a neighboring one is selected. This also means that when calibrating the station, none of the signal processing discussed in this document may be used.

Furthermore, the location of the antennas needs to be known to a certain degree. The error in distance between the elements may not be larger than about 60 degrees of phase rotation. When this is achieved, the resulting calibration results can be used for a wide range of frequency bands, instead of just one.

One other disadvantage of this technique is the necessity for a well defined point source. On the low frequencies a LOFAR station is observing, this may very well be a problem. The station calibration considerations are explored in detail in [17].


### 1.5.3 Radio Frequency Interference (RFI)

There are two main reasons to do beamforming at the remote station. On the one hand we can reduce the amount of data to be transported considerably, but on the other hand beamforming opens the possibility to spatially filter out interfering signals.

Radio Frequency Interference (RFI) is one of the greatest risks associated with the LOFAR project. The frequency ranges in which we are interested are infested with interference. We need to be able to filter out large portions of this interference at the station level if we are to be successful.

Using the beamformer we will be able to spatially filter out a limited number of interfering sources. The spatial filtering in the beamformer works parallel to spectral filtering using two cascaded filterbanks both at the input and at the output of the digital beamformer.

The reason we use two cascaded filterbanks is that we need to reduce the bandwidth of the beamformer input so we have a relatively narrowband signal to beamform, but we don't have the computational power to go to 1 kHz channels, the desired output bandwidth of the LOFAR station, directly.

Author: P.C. Broekema	Date of issue: 2004-May-16 Kind of issue: Limited	Scope: Project documentation Doc.nr.: LOFAR-ASTRON-MEM-136	
	Status: For Review Revision nr.: 1.0	File: <a href="http://dop47.nfra.nl/chris/Thesis/Thesis.pdf">http://dop47.nfra.nl/chris/Thesis/Thesis.pdf</a>	

## 2 Background information

### 2.1 Coordinate systems

A LOFAR station will consist of a number of receiving elements which will work together as a phased array. The position of these elements can be defined in Cartesian  $x$ ,  $y$  and  $z$  coordinates as is shown in figure 2.1[16]. The  $x$ -axis will be pointed North, the  $y$ -axis to the West. For the purpose of this thesis it will often be convenient to specify the location of the elements relative to the center of the array. These will be denoted as  $px$ ,  $py$  and  $pz$ , although the latter is often disregarded.

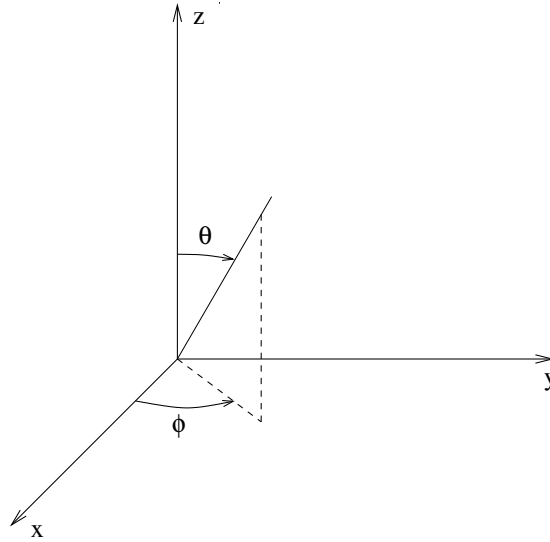


Figure 3: Coordinate systems for the antenna positions with respect to the LOFAR station

The direction of propagation, which is parallel to the direction of arrival of incoming radiation, is specified in terms of a zenith angle  $\theta$  and an azimuth angle  $\phi$ . This is also shown in figure 2.1. The relation of  $\phi$  and  $\theta$  to the azimuth  $az$  and the elevation  $el$  is defined by [16]:


$$\theta = 90^\circ - el \quad (1)$$

$$\phi = -az \quad (2)$$

The direction of arrival can also be defined in terms of the directional cosines:

$$\rho = \sin \theta \cos \phi = \cos(el) \cos(az) \quad (3)$$

$$\sigma = \sin \theta \sin \phi = -\cos(el) \sin(az) \quad (4)$$

Author: P.C. Broekema	Date of issue: 2004-May-16 Kind of issue: Limited	Scope: Project documentation Doc.nr.: LOFAR-ASTRON-MEM-136	
	Status: For Review Revision nr.: 1.0	File: <a href="http://dop47.nfra.nl/chris/Thesis/Thesis.pdf">http://dop47.nfra.nl/chris/Thesis/Thesis.pdf</a>	

## 2.2 Introduction of basic concepts

### 2.2.1 Sensitivity

The sensitivity of an antenna, or an antenna array is a measure for the least powerful signal that can still be detected with the device.

When defining the sensitivity of an array, we first need a measure for the antenna performance. Radio astronomers find it convenient to express the power of various signals from a radio telescope in terms of equivalent temperature  $T$ . The noise introduced by the *system* of a single antenna is expressed as  $T_{sys}$  and contains contributions from the receiver noise, feed losses, spillover, atmospheric emissions, galactic background and cosmic background noise[14]. It is often instructive to express the system temperature in terms of the system equivalent flux density, or SEFD, defined as the flux density of a source that would deliver the same amount of power:

$$SEFD = \frac{T_{sys}}{K} \quad (5)$$

where  $K = (\eta_a A)/(2k_B)$ ,  $\eta_a$  is the antenna efficiency,  $A$  is the antenna area and  $k_B = 1.380 \times 10^{23} \text{ Joule } K^{-1}$  is the Boltzman constant. The sensitivity of an single-polarization image formed from a homogeneous array built with  $N$  identical elements is (in Jansky)[14]:


$$\Delta I_m = \frac{1}{\eta_s} \frac{SEFD}{\sqrt{N(N-1)} \Delta \nu t_{int}} \quad (6)$$

$\Delta \nu$  is the observing bandwidth and  $t_{int}$  is time over which is integrated. The system efficiency is expressed in the factor  $\eta_s$ . The Jansky is a measure for the sensitivity of an image and is defined as  $1 \text{ Jansky} = 1 \text{ Jy} = 10^{-26} \text{ W m}^{-2} \text{ Hz}^{-1}$ .

All this shows us that the sensitivity of the array is largely defined by the the number of elements  $N$ . Recall the layout of the LOFAR array as seen in figure 2. Since location of the elements does not affect the resulting sensitivity of the array, most elements are placed in a location near the center of the array. This reduces the distance the bulk of the data needs to travel before reaching the central processing core. This in turn reduces total cost of the instrument.

### 2.2.2 Resolution

For every instrument we build, the resulting image will be blurred and we cannot distinguish details smaller than a certain limit called the *resolution* of our instrument. This is not unique to astronomical devices, all imaging devices have a fundamental resolution limit below which object points cannot be distinguished.[6]. The resolution of an array depends directly on the size of the array relative to the wavelength of the observed frequency. The angle of incidence,  $\alpha$ , is also a limiting factor resolution wise.

Author: P.C. Broekema	Date of issue: 2004-May-16 Kind of issue: Limited	Scope: Project documentation Doc.nr.: LOFAR-ASTRON-MEM-136	
	Status: For Review Revision nr.: 1.0	File: <a href="http://dop47.nfra.nl/chris/Thesis/Thesis.pdf">http://dop47.nfra.nl/chris/Thesis/Thesis.pdf</a>	

The unusually low frequencies, and therefore large wavelengths, LOFAR is targeted at, have as a direct consequence that the maximum baseline of the array needs to be quite large. Fortunately the number of elements on the outside edge of the array has limited influence on the resulting resolution. In figure 2 we see that although the total instrument is quite large, only a relatively small number of antenna fields is placed outside a central area of only a few kilometers in diameter.

### 2.2.3 Beamforming and delay compensation

An antenna array gathers it's signals by combining all outputs of the elements in a single signal. Un-weighted addition of the signals would, in case of a perfect system, cause the array to look straight up, but by introduction of specific time delays in the antenna outputs we are able to point the beam in any direction. In figures 4 and 5 we see these concepts demonstrated.

For small time delays, adding specific phase delays to the signal has an equivalent effect. Advantage is that adding a phase delay is easier, and therefore cheaper, to accomplish than adding a physical time delay to the signal. Phase delays are however frequency dependent, introducing a number problems. One of these is beam squint, which will be introduced in section 2.2.9. When phase delays are used, the resulting array is commonly known as a *phased array*. The frequency dependency of such a phased array means that it is only completely accurate on relatively narrow band signals.

The complex phase delays for element  $n$  located at  $(px(n), py(n))$ , pointing to  $(\phi, \theta)$  can be determined using [11]:

$$w(n) = e^{(-2i\pi(px(n) \sin(\theta) \cos(\phi) + py(n) \sin(\theta) \sin(\phi)))} \quad (7)$$


By applying 7 to each element in the array, we can determine the steer vector  $\mathbf{w}$  for the beamformer. The beamformer on the signal vector  $\mathbf{x}$  at time  $t$  can now be described as [11]:

$$y(t) = \mathbf{w}^H \mathbf{x}(t) \quad (8)$$

where the superscripted H denotes the Hermitian or complex conjugate transpose.

### 2.2.4 Adaptive beamforming

Conventional beamformers use a static weight vector which only depends on the required looking direction, the array configuration and the observed frequency. It is however possible to automatically recalculate the weightvector to minimize the influence of interference in the signal. This is called adaptive beamforming.

Author: P.C. Broekema	Date of issue: 2004-May-16 Kind of issue: Limited	Scope: Project documentation Doc.nr.: LOFAR-ASTRON-MEM-136	
	Status: For Review Revision nr.: 1.0	File: <a href="http://dop47.nfra.nl/chris/Thesis/Thesis.pdf">http://dop47.nfra.nl/chris/Thesis/Thesis.pdf</a>	

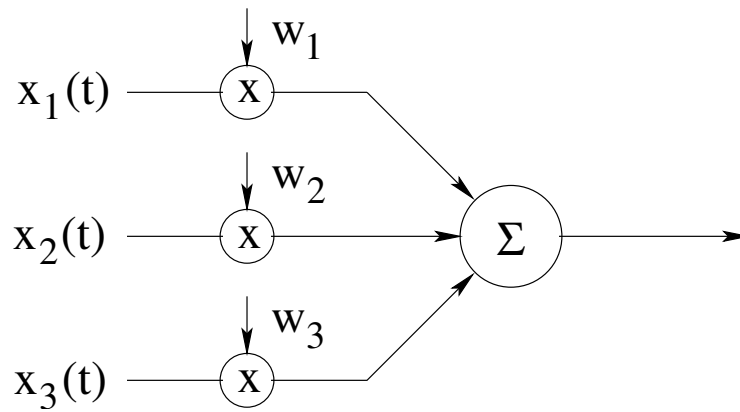


Figure 4: Concept of a conventional beamformer

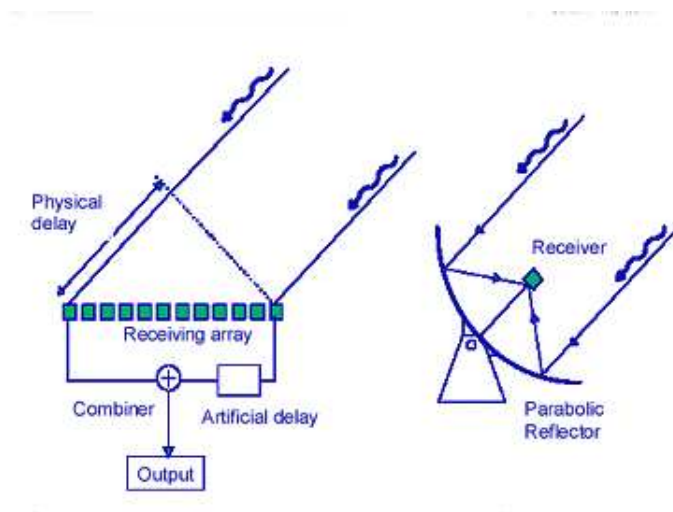



Figure 5: Steering using delay compensation



Author: P.C. Broekema	Date of issue: 2004-May-16 Kind of issue: Limited	Scope: Project documentation Doc.nr.: LOFAR-ASTRON-MEM-136	
	Status: For Review Revision nr.: 1.0	File: <a href="http://dop47.nfra.nl/chris/Thesis/Thesis.pdf">http://dop47.nfra.nl/chris/Thesis/Thesis.pdf</a>	

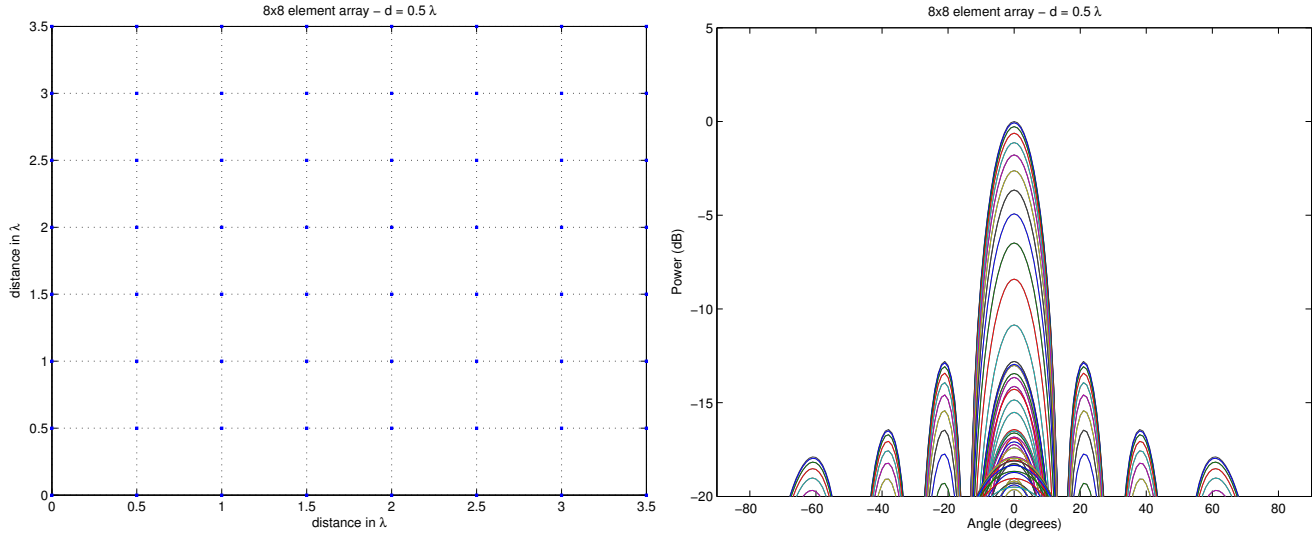


Figure 6: Array configuration and beamshape of a regular array,  $d = \frac{1}{2}\lambda$ . The colored lines in the right hand picture represent beamshapes at various positions on the axis on which we have projected this picture, thus giving us an impression of the whole beamshape in a two dimensional figure.

### 2.2.5 Beam shape

The beamshape of a particular beamformer is defined as being the sensitivity (gain) of the beamformer as a function of looking direction. The beamshape is normally expressed in dB relative to the highest gain, or the beam top. Figure 6 shows the beamshape for a 64 element square array. Please note that the distance between elements is  $\frac{1}{2}\lambda$ .  $\lambda$  is the wavelength of the signal and is defined as:


$$\lambda = \frac{c}{f} \quad (9)$$

$f$  is the frequency of the signal and  $c$  is the speed of light. The figure shows the beam from it's side, with the lines representing the relative power of the beam for several positions on the axis on which we have projected this picture.

The width of the half power beam, or the contour of the  $-3dB$  beam top, is called the half power beamwidth (HPBW) and is approximated by[6]

$$HPBW \approx \frac{\lambda}{D}. \quad (10)$$

Here  $\lambda$  is the wavelength of the observed frequency or, for wider band signals, the center of the observed frequency band.  $D$  is the aperture size of the array, which is the maximum distance between two elements of the array.

Author: P.C. Broekema	Date of issue: 2004-May-16 Kind of issue: Limited	Scope: Project documentation Doc.nr.: LOFAR-ASTRON-MEM-136	
	Status: For Review Revision nr.: 1.0	File: <a href="http://dop47.nfra.nl/chris/Thesis/Thesis.pdf">http://dop47.nfra.nl/chris/Thesis/Thesis.pdf</a>	

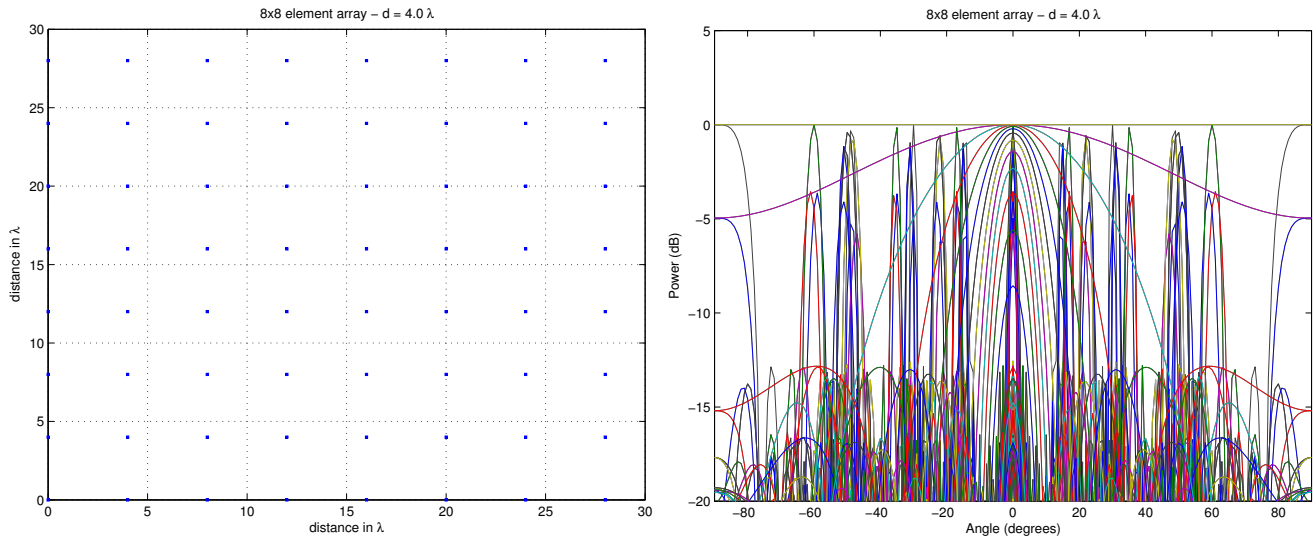


Figure 7: Array configuration and beamshape of a regular array,  $d = 4\lambda$ .

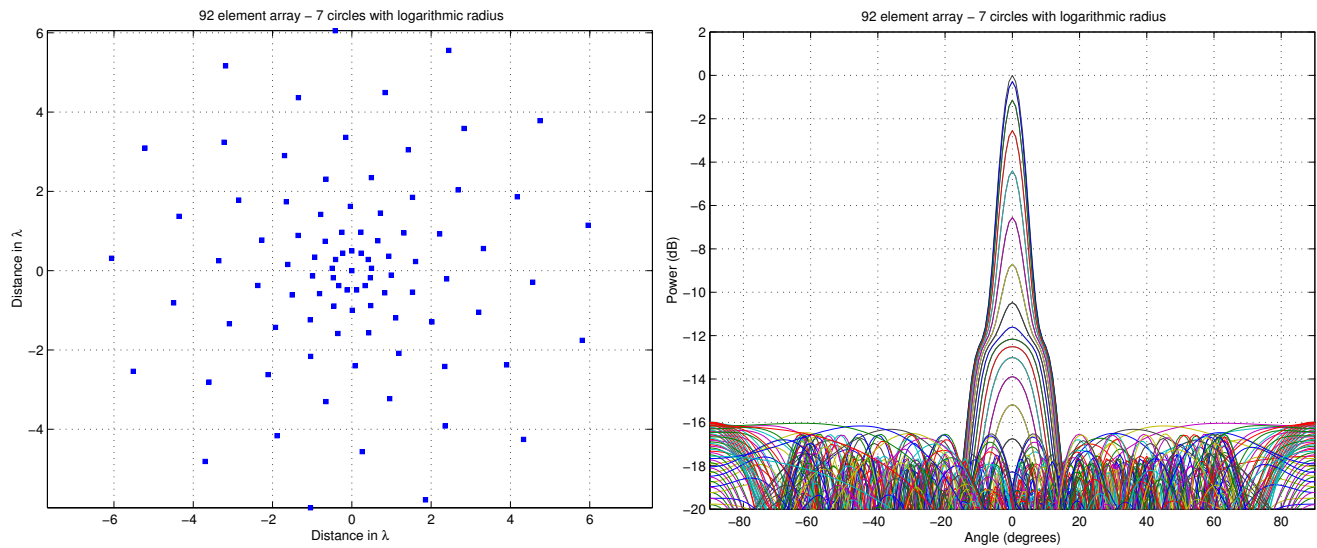



Figure 8: Array configuration and beamshape of an irregular array.

Author: P.C. Broekema	Date of issue: 2004-May-16 Kind of issue: Limited	Scope: Project documentation Doc.nr.: LOFAR-ASTRON-MEM-136	
	Status: For Review Revision nr.: 1.0	File: <a href="http://dop47.nfra.nl/chris/Thesis/Thesis.pdf">http://dop47.nfra.nl/chris/Thesis/Thesis.pdf</a>	

### 2.2.6 Side lobes

Looking back at figure 6 we see that it shows several peaks. Apart from the main lobe aimed at the zenith, it also shows several smaller peaks, called side lobes. Side lobes are a natural property of antenna arrays caused by coherent addition of antenna signals in a particular direction.

### 2.2.7 Grating lobes - regular arrays

As mentioned before, LOFAR will observe at a frequency range between 10 and 250 MHz. Equation 9 tells us that the wavelength of the signals we want to observe varies between 1.2 and 30 meters. Classic beamforming literature insist that spacing between elements of the array should not exceed  $\frac{1}{2}\lambda$ . This is known as the *Shannon criterion*.

Spacing the elements this close together is not a viable option for LOFAR, this would require far too many antennas to be practical. Therefore the LOFAR stations will be violating this criterion. This means that, for at least a significant part of the observed spectrum, quite powerful grating lobes will appear in the beampattern.[8][11] Grating lobes are unique to array receivers and are caused by regular, periodic spacing of the array elements.


This phenomenon is illustrated in Figures 6 and 7. As mentioned before, figure 6 is a sideview of the beampattern of a regular array which does adhere to the Shannon criterion. The resulting beam is nicely shaped with only the sidelobes to take into account.

Figure 7 however shows the same array, only now the elements are spaced  $4\lambda$  from each other. The resulting grating lobes are so powerful that they rival the main lobe in power. This clearly is not acceptable for a LOFAR station.

### 2.2.8 Grating lobes - irregular arrays

Since grating lobes are caused by the regular and periodic spacing of array elements, we propose to use a irregular configuration to prevent the grating lobes from appearing. The result of one such configuration can be seen in figure 8. This is an array consisting of seven concentric rings, with a logarithmically increasing diameter. The array looks quite regular, but the logarithmic spacing of the rings makes sure there is no regular periodic spacing of the elements. The resulting beampattern shows no evidence of grating lobes, and even the sidelobes are markedly less powerful.

There are however some disadvantages to this approach. Classic beampatterns using regular arrays were quite easily analyzed mathematically. The beamshape resulting from an irregular array cannot be described with a closed expression. Mathematical analysis is therefore far more difficult. This forces us to use simulation instead of mathematical analysis to verify the station beamformer design.

Author: P.C. Broekema	Date of issue: 2004-May-16 Kind of issue: Limited	Scope: Project documentation Doc.nr.: LOFAR-ASTRON-MEM-136	
	Status: For Review Revision nr.: 1.0	File: <a href="http://dop47.nfra.nl/chris/Thesis/Thesis.pdf">http://dop47.nfra.nl/chris/Thesis/Thesis.pdf</a>	

Some higher level algorithms that may be used at the LOFAR central core, also require some level of regularity in the array to function. While (pseudo) random arrays may pose a problem in this respect, we are confident the array presented here contains enough regularity. It must be mentioned that the 92 element array presented here is by no means the only answer. Most arrays without repeating baselines should give comparable performance. Proposed array configurations for the LOFAR Initial Test Station contain five logarithmically spaced spiral arms, performing about the same.

### 2.2.9 Beam squint

Array bandwidth can be limited by the bandwidth of the elements in the array, but often the more severe limitation is caused by the use of complex phase shifters to scan the beam instead of time-delay devices. Since phase delays are frequency dependent, the peak is scanned to the desired angle only at the center frequency  $f_0$ . Otherwise we will observe pattern squint, in which the beam peak angle is reduced for frequencies below the design frequency as is shown in figure 9. This clearly shows the squint effect in the red line when the beam is pointed away from the zenith. Also note the change in sidelobe levels and locations.

A three dimensional squint effect is illustrated in figure 10. Here we see two beampatterns, one without beamsquint, and one where the difference in observed frequency and center frequency causes the pointing direction to be higher than expected. The beam was aimed at the point denoted with an asterisk.

Since beamsquint effects are more pronounced at lower frequencies, we need to take a careful look at these effects. Most studies of beamsquint have concentrated on regular and non-sparse arrays, so the actual effects we will encounter are not really known. If there are effects to consider, they will most likely cause significant pointing errors, especially in the lower frequency ranges.

The way in which the adaptive beamforming techniques are affected by beam squint is largely unknown.

## 2.3 Interference subspace estimation and spatial projection

Phased array technology is relatively new. In recent years several techniques have been developed to adaptively modify the beam characteristics to suppress interfering signals in the input. The availability of these adaptive nulling techniques to combat RFI, which is a growing problem in radio astronomy, is one of the main advantages of using phased arrays for a new generation of radio telescope. Perhaps the best known approach to adaptive nulling for phased arrays is constrained power minimization, using algorithms such as Minimum Variance (MV).

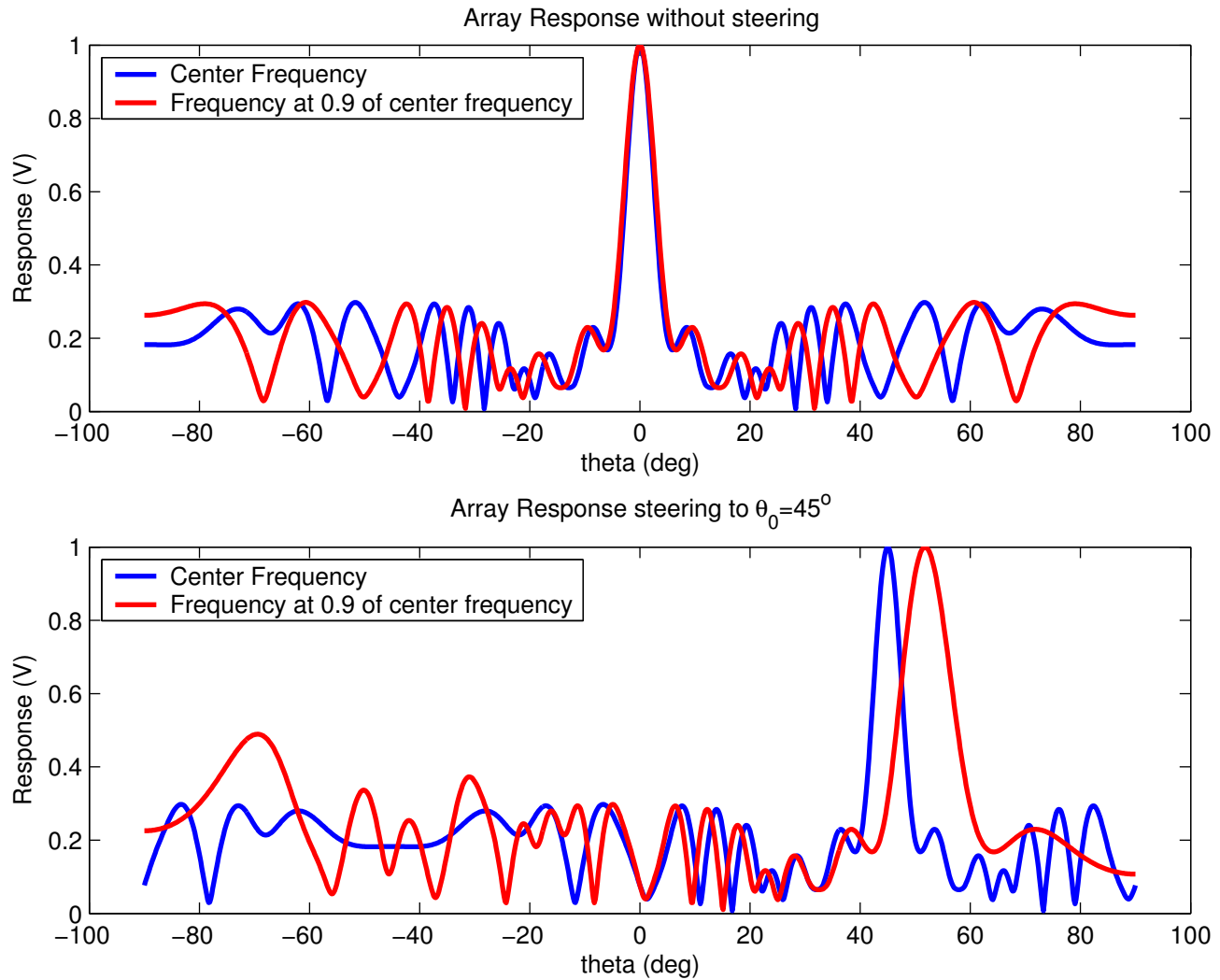



Figure 9: These two figures show the array response for two signals when looking at the zenith (top) and when pointed at  $\theta = 45^\circ$  off the zenith (bottom). The bottom picture clearly shows that the beam will be offset slightly when observing a frequency other than the center frequency used for the weightvector calculation. This is called the beam squint effect.

Author: P.C. Broekema	Date of issue: 2004-May-16 Kind of issue: Limited	Scope: Project documentation Doc.nr.: LOFAR-ASTRON-MEM-136	
	Status: For Review Revision nr.: 1.0	File: <a href="http://dop47.nfra.nl/chris/Thesis/Thesis.pdf">http://dop47.nfra.nl/chris/Thesis/Thesis.pdf</a>	

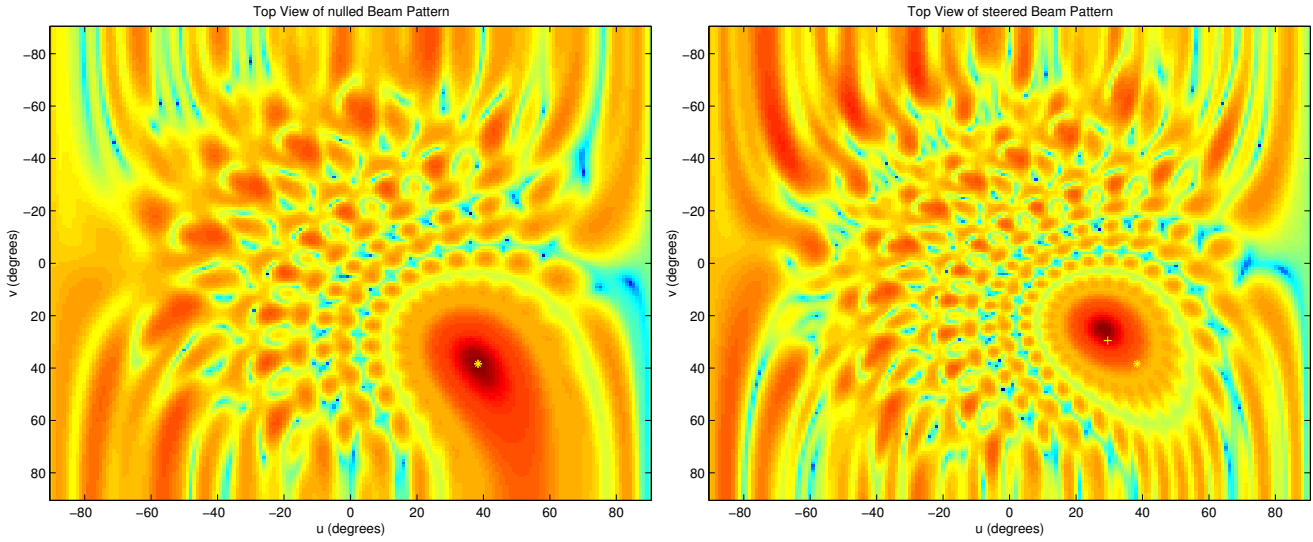


Figure 10: In the left beampattern, the observed frequency and the frequency used to aim the beam are the same. The result is a beam aimed exactly where we expect it to be (the yellow asterisk). In the right hand picture the observed frequency is higher than the center frequency used to aim the beam. The result is beam squint. We can see the beam aimed higher than the yellow asterisk, which is the expected location of the beam top.


### 2.3.1 Minimum variance

The detailed specification and implementation of the Minimum variance technique is discussed in detail in [5] and [4] and shall not be repeated here. The main conclusion must be however that Minimum Variance is not suitable for radio astronomy applications. This has several reasons. First of all the depth of the resulting nulls is directly proportional to the interference-to-noise ratio (INR). This is no problem for many communication and radar applications, but for astronomical signals, which require long integration times to detect, this means that intermittent signals may have a INR much less than 1 and yet be orders of magnitude stronger than the desired signal. This has the potential to wreck the results for that integration period. MV is ineffective against such interference.

Secondly, MV is subject to a phenomenon known as *weight jitter* or *pattern rumble*. MV relies on inversion of the array correlation matrix  $R$ , which is defined as the expected value of the outer product

$$\hat{R} = \sum \mathbf{x}(t)\mathbf{x}(t)^H \quad (11)$$

$R$  also contains information about the noise, which is represented in the low-order Eigen values of  $R$ . Inversion causes the noise Eigen values to become large, allowing the noise Eigen vectors to make a significant contribution to the calculated weights. Since the noise Eigen vectors are effectively random, this may cause considerable variance between updates, even in the main beam.


Author: P.C. Broekema	Date of issue: 2004-May-16 Kind of issue: Limited	Scope: Project documentation Doc.nr.: LOFAR-ASTRON-MEM-136	
	Status: For Review Revision nr.: 1.0	File: <a href="http://dop47.nfra.nl/chris/Thesis/Thesis.pdf">http://dop47.nfra.nl/chris/Thesis/Thesis.pdf</a>	

### 2.3.2 Estimating the Interference subspace

For MV the disadvantages discussed above can be traced to the use of the entire matrix  $R$  instead of using only the interference subspace to calculate the adaptive weights. An alternative approach is to explicitly estimate the interference subspace and then calculate weights corresponding to beams in the orthogonal complement of this subspace. This method of forming nulls is called *spatial projection*[4]. A straightforward implementation is to compute an estimate of  $R$  as in MV and then identify the interference subspace using an Eigen decomposition. For large arrays both the computation of  $R$  and the Eigen decomposition are computationally very demanding.

### 2.3.3 Subspace Tracking

To mitigate the computational load of the Eigen decomposition we can use a subspace tracking technique[10]. Using a tracking technique we can find Eigen vectors and values on a sample by sample basis without the need to explicitly estimate  $R$ , thus reducing computational demands drastically. It has been demonstrated that the use of a subspace tracking technique combined with spatial projection is viable alternative to direct Eigen decomposition[4][7].

Author: P.C. Broekema	Date of issue: 2004-May-16 Kind of issue: Limited	Scope: Project documentation Doc.nr.: LOFAR-ASTRON-MEM-136	
	Status: For Review Revision nr.: 1.0	File: <a href="http://dop47.nfra.nl/chris/Thesis/Thesis.pdf">http://dop47.nfra.nl/chris/Thesis/Thesis.pdf</a>	

### 3 Array Processing techniques

Figure 11 shows the basic components of the LOFAR station signal processing chain. Although the design and implementation of the filterbanks fall outside the scope of this thesis, they do give us the ability to influence the bandwidth of the beamformed signal. For the moment we can assume the filterbanks to perform like a Fourier transform. The total signal bandwidth divided by the number of transform points of the first filterbank defines the input bandwidth of beamformer.

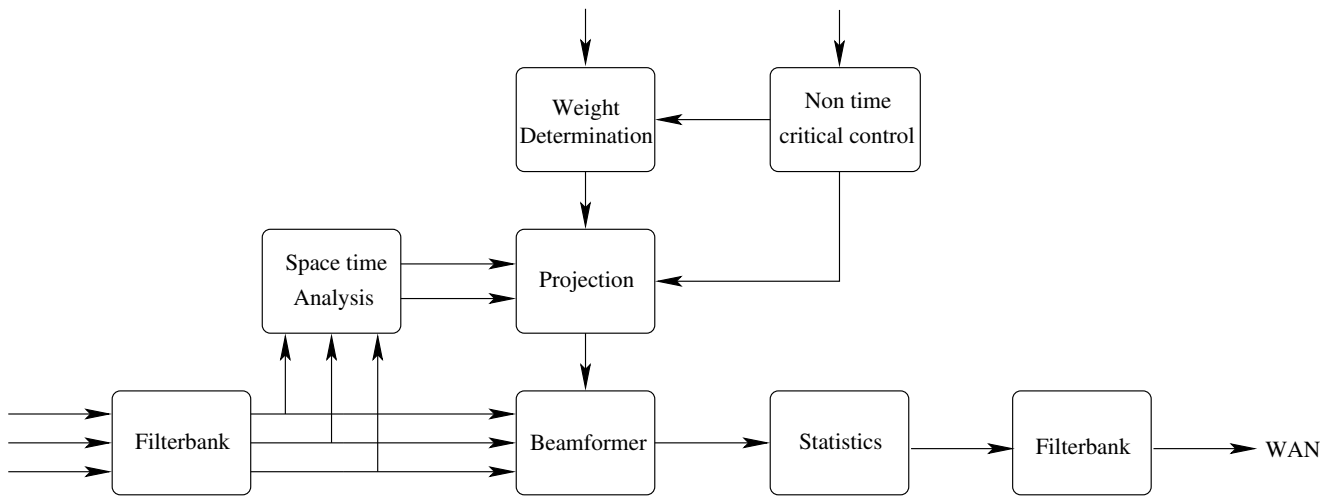



Figure 11: Application model of the LOFAR digital station beamformer

The beamformer applies the weights calculated in the projection block. These weights are calculated using the direction vectors for the looking direction and any interfering signals as provided by the weight determination block (looking direction) and the space time analysis block (interferers). Non time critical control provides the beamformer with parameters like looking direction, subband selection and array configuration. These parameters are, like the name suggests, non time critical in nature.

#### 3.1 Deterministic suppression

Many interfering signals are well known and fairly static transmitters like for instance a radio station. Such static sources can be suppressed by introducing a deterministic null at the known location. A steervector is calculated for the interferer, using the beamformer equations mentioned in section 2.2.3. This is a primitive way to spatially filter a source with predictable results. It is not very flexible however, since operator interaction is needed to add or change an interferer location.



Author: P.C. Broekema	Date of issue: 2004-May-16 Kind of issue: Limited	Scope: Project documentation Doc.nr.: LOFAR-ASTRON-MEM-136	
	Status: For Review Revision nr.: 1.0	File: <a href="http://dop47.nfra.nl/chris/Thesis/Thesis.pdf">http://dop47.nfra.nl/chris/Thesis/Thesis.pdf</a>	

## 3.2 Automatic detection techniques

### 3.2.1 Eigen value based techniques

Eigen value decompositions are standard matrix operations that are well understood and for which efficient implementations are widely available. For the exact mathematical definition I refer to any book on linear algebra. Several numerical implementations can be found in [12].

The array correlation matrix (ACM), as introduced in section 2.3.1, for an array of  $K$  elements is defined as:

$$\hat{\mathbf{R}} = \frac{1}{K} \sum_{k=1}^K \mathbf{x}(t_k) \mathbf{x}(t_k)^H \quad (12)$$

This assumes that the entire signal matrix  $\mathbf{x}$  is known. The ACM can be estimated over a number of snapshots using:


$$\hat{\mathbf{R}}(t_k) = \alpha \mathbf{x}(t_k) \mathbf{x}^H(t_k) + (1 - \alpha) \hat{\mathbf{R}}(t_{k-1}), \text{ where } 0 < \alpha < 0.1 \quad (13)$$

The factor  $\alpha$  is known as the forgetting factor, with which the older snapshots are weighted less than the newer ones. The forgetting factor also dictates the maximum number of snapshots used in the estimation. The range of  $\alpha$  in equation is a bit arbitrary, but experiments have shown this to yield a reasonable estimate.

### 3.2.2 Projection Approximation Subspace Tracking with deflation

An indirect approach to obtaining the Eigen vectors and values, is the Projection Approximation Subspace Tracking with deflation (PASTd) technique[18]. This technique doesn't require computation of an ACM, both of which require considerable computational resources. Instead it estimates the Eigen values and vectors on a snapshot by snapshot basis. It does however require a significant number of snapshots to obtain an accurate estimate. The increase in required snapshots is a factor ten initially, but thereafter the algorithm naturally *tracks* the Eigen vectors using a much smaller number of snapshots.[7]

A basic description in pseudo code is as follows, where  $N_{Eigen}$  is the number of required Eigen vectors. Note that the number of required Eigen vectors is equal to the number of interfering sources to be nulled. Assume for now that this number is known, in section 3.3 we will introduce some possible techniques to estimate this number.

Author: P.C. Broekema	Date of issue: 2004-May-16 Kind of issue: Limited	Scope: Project documentation Doc.nr.: LOFAR-ASTRON-MEM-136	
	Status: For Review Revision nr.: 1.0	File: <a href="http://dop47.nfra.nl/chris/Thesis/Thesis.pdf">http://dop47.nfra.nl/chris/Thesis/Thesis.pdf</a>	

1. Obtain  $N$  snapshots,  $\mathbf{x}_1$  to  $\mathbf{x}_N$
2. Calculate the Eigen vectors,  $\mathbf{w}_r$  and values,  $d(r)$ , using PASTd. Initialize  $\mathbf{w}_r$  with ones:

```

for  $n = 1$  to  $N$ 
     $a_n = x_n$ 
    for  $r = 1$  to  $N_{Eigen}$ 
         $y = \mathbf{w}_r^H \mathbf{a}_n$ 
         $d = \beta d + |y|^2$ 
         $\mathbf{e} = \mathbf{x}_n - \mathbf{w}_r y$ 
         $\mathbf{w}_r = \mathbf{w}_r - \mathbf{e} \left( \frac{y}{d} \right)'$ 
         $\mathbf{a}_n = \mathbf{a}_n - \mathbf{w}_r y$ 

```


One of the additional advantages of the PASTd technique is the fact that it does not require any special mathematical functions to implement it. As a result the algorithm has a lower operations count, but as we have seen requires many more snapshots than the Eigen Value Decomposition techniques described in section technique 3.2.1.

Experiments carried out by the THousand Element Array (THEA, part of the Square Kilometer Array (SKA) effort) project team showed that approximately three to four times as many snapshots were needed to obtain the same level of Eigen vector convergence using PASTd compared to direct EVD.[7] However, Yang predicts that the PASTd algorithm can quickly adapt to changes in the input space, effectively tracking the interfering source.[18] Note that the Eigen values produced by the PASTd algorithm have a different weighting to those of the EVD[7]. This is important to realize when trying to determine the number of interfering sources in a signal.

The results of the PASTd algorithms depend on the  $\beta$  chosen parameter. This behaves like a logarithmic forgetting factor. Normally this would be chosen in the range  $0.95 < \beta < 1$  which corresponds to a window of significant snapshots varying from 20 to  $\infty \left( \frac{1}{1-\beta} \right)$ . Increasing  $\beta$  results in a longer window with more significant snapshots. This allows less powerful signals to be tracked at a cost of a slower converging algorithm. Lower values of  $\beta$  can cause the algorithm to become unstable, although convergence is faster.

PASTd is able to update the signal Eigen vectors and Eigen values every update. It delivers a *nearly* orthonormal Eigen vector estimate. Although we don't need a perfectly orthonormal Eigen vector estimate, we do need to guard against excessive drift of the estimate. Measuring the orthogonality of the estimate is a relatively easy way to estimate the accuracy of the PASTd algorithm. We do need to realize that the spatial projection technique we will introduce in section 3.4.1 assumes that the input vectors are orthonormal. Non-orthonormal Eigen vectors from the PASTd algorithm will introduce an error in the nulling direction.

We would expect the PASTd algorithm to react quite well to small changes in the signal space (i.e.

Author: P.C. Broekema	Date of issue: 2004-May-16 Kind of issue: Limited	Scope: Project documentation Doc.nr.: LOFAR-ASTRON-MEM-136	
	Status: For Review Revision nr.: 1.0	File: <a href="http://dop47.nfra.nl/chris/Thesis/Thesis.pdf">http://dop47.nfra.nl/chris/Thesis/Thesis.pdf</a>	

moving interfering sources). The appearance of a new source however would require the algorithm to reconverge. Depending on the chosen  $\beta$  this could take several hundred snapshots to achieve[7].

### 3.3 Determine the number of sources

#### 3.3.1 Thresholding

We assume that the adaptive beamformer will be based on an Eigen value technique. This class of techniques results in a set of Eigen vectors, describing the position of the source in relation to the array, and a number of Eigen values, which represent the power of the source. As such, one of the most obvious ways to determine the number of sources in the antenna signals is thresholding. Simply put, this involves counting any Eigen value above a certain threshold as a RFI source. The value of the threshold should be determined experimentally.

#### 3.3.2 Minimum Description Length (MDL)

Minimum description length is an algorithm to determine the number of interfering sources in a set of Eigen values. The MDL technique is based on the perception that each model can be perceived as encoding the observed data and that the optimum model is the one model that yields the minimum code length. In this case this means selecting the model for which a specific criterion is minimized[10]. An estimate for the number of sources is that value of  $\hat{N}_S$ , which minimizes this criterion.

Experiments done previously by the SKA team and more recently using my own software have shown that PASTd Eigen values are weighted differently than normal. We should investigate this to determine if PASTd Eigen values can be used in combination with MDL. Experiments in Matlab have shown that without post-processing the Eigen values from PASTd will not result in correct answers using MDL. This means we may have to periodically use a real Eigen value decomposition to estimate the number of interferers in the signal. This is not necessarily a problem, since we can at the same time verify the accuracy of the PASTd tracking algorithm

### 3.4 RFI suppression techniques

#### 3.4.1 Spatial Projection

Consider the conventional beamformer as defined in section 2.2.3. Here,  $\mathbf{w}$  is a vector of weights, also known as the steering vector, which is selected so as to maximize the output  $y(t)$  in a given direction.  $\mathbf{x}(t)$  is the vector of antenna outputs. Assuming we have knowledge of steering vectors associated with

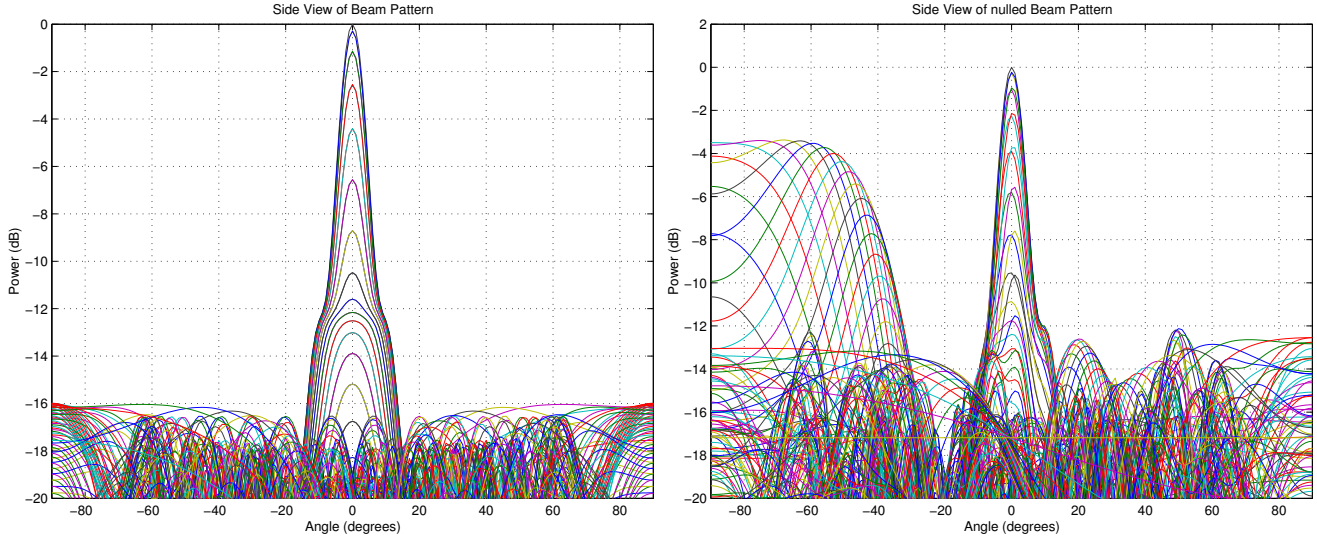


Figure 12: Side view of a normal beamshape and one distorted by a null in a sidelobe

interfering signals, a simple procedure to introduce desired nulls is to pre-filter  $\mathbf{x}(t)$  before beamforming; i.e., compute

$$\mathbf{x}_F(t) = \mathbf{P}_{\mathbf{W}}^{\perp} \mathbf{x}(t), \quad (14)$$

where  $\mathbf{P}_{\mathbf{W}}^{\perp}$  is the  $N \times N$  projection matrix. This is defined as:


$$\mathbf{P}_{\mathbf{W}}^{\perp} = \mathbf{I} - \mathbf{W}(\mathbf{W}^H \mathbf{W})^{-1} \mathbf{W}^H, \quad (15)$$

with  $\mathbf{W}$  being the  $N \times k$  matrix formed by concatenating the  $k$  Direction Of Arrival (DOA) vectors  $\mathbf{w}_1 \dots \mathbf{w}_k$ . The resulting weight vector  $\mathbf{w}_p$  is used in the beamformer in the normal way, with  $\mathbf{w}_p = \mathbf{P}_{\mathbf{V}}^{\perp} \mathbf{w}$ .

The resulting algorithm lacks any means to protect the main beam from the orthogonal projections. Depending on the location of the projected null, distortions in main beam shape can be quite severe.

Nulls produced by the spatial projection technique dependent on direction of the interferer and to a lesser extend, array configuration (through the interference steering vectors). In contrast to other nulling algorithms, such as Minimum Variance [5] where the depth of the nulls depend on the power of the interfering signal, this technique will always produce a null of infinite depth.[7]

The fact that nulls are exceedingly deep, causes quite severe distortions in the main beam when nulls are placed near the main lobe, or a side lobe. This is illustrated in Figures 12 and 13. We need to make sure that adding nulls to our signal does not degrade the beam to such a degree that it becomes unusable.

Author: P.C. Broekema	Date of issue: 2004-May-16 Kind of issue: Limited	Scope: Project documentation Doc.nr.: LOFAR-ASTRON-MEM-136	
	Status: For Review Revision nr.: 1.0	File: <a href="http://dop47.nfra.nl/chris/Thesis/Thesis.pdf">http://dop47.nfra.nl/chris/Thesis/Thesis.pdf</a>	

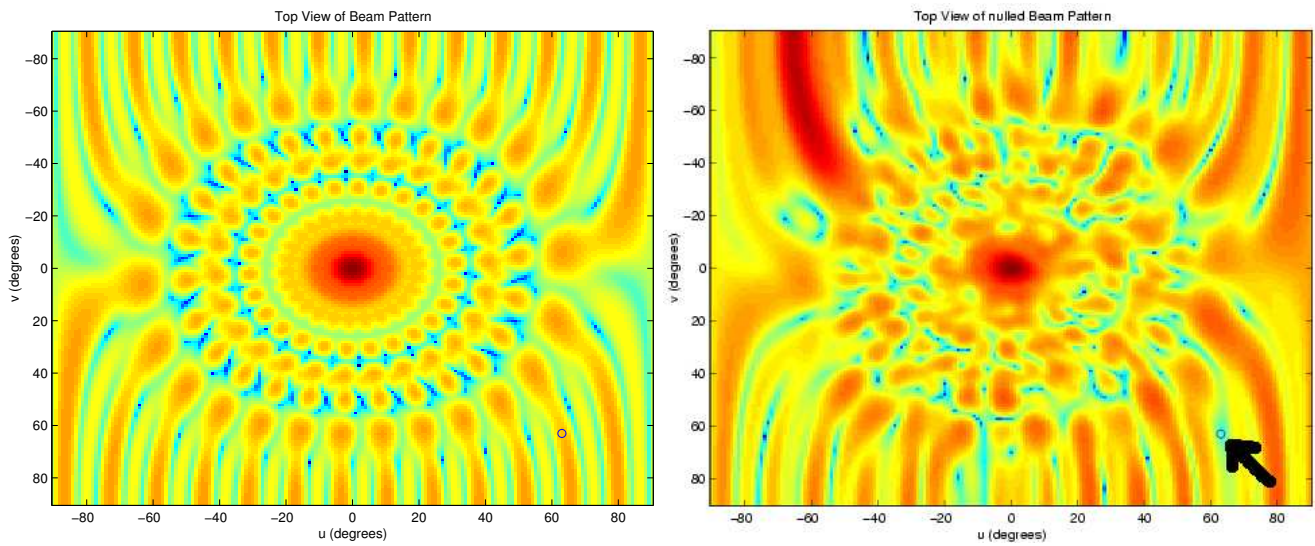



Figure 13: Same situation as 12, now viewed from the top. The 'o' marks the null.

Author: P.C. Broekema	Date of issue: 2004-May-16 Kind of issue: Limited	Scope: Project documentation Doc.nr.: LOFAR-ASTRON-MEM-136	
	Status: For Review Revision nr.: 1.0	File: <a href="http://dop47.nfra.nl/chris/Thesis/Thesis.pdf">http://dop47.nfra.nl/chris/Thesis/Thesis.pdf</a>	

## 4 Development of simulation environment

Both incarnations of the remote station simulation use the same basic model. This application model is shown in figure 11 which was already introduced in section 3. It shows the basic components of the LOFAR remote station.

### 4.1 Simulation environment

#### 4.1.1 Matlab - StationGUI

Matlab was used to develop a basic simulation of the LOFAR remote station functionality. This includes filterbanks, an adaptive beamformer and an advanced data generator. The complete simulation has a graphical frontend shown in figure 14.

This Matlab simulation was used to gain experience in the way the various algorithms interact with each other and in the problems connected with the implementation and configuration of the various components. Since Matlab is not capable of processing large amounts of data, the scale of the simulations is a lot smaller.

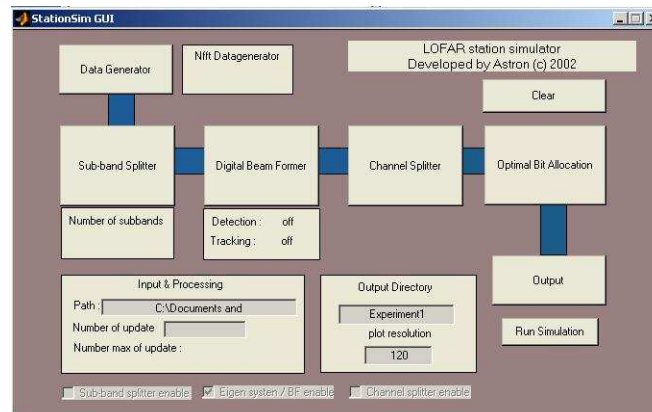



Figure 14: Main configuration window of the Matlab simulation

#### 4.1.2 C++ StationSim

The inability of Matlab to process large amounts of data motivated the development of a C++ simulator of the LOFAR remote station. This also includes filterbanks, adaptive beamformer and an advanced signal generator. Special care was taken to develop the C++ simulation along the same lines as the parallel Matlab simulation. The finished product is capable of reading configuration files generated by

Author: P.C. Broekema	Date of issue: 2004-May-16 Kind of issue: Limited	Scope: Project documentation Doc.nr.: LOFAR-ASTRON-MEM-136	
	Status: For Review Revision nr.: 1.0	File: <a href="http://dop47.nfra.nl/~chris/Thesis/Thesis.pdf">http://dop47.nfra.nl/~chris/Thesis/Thesis.pdf</a>	

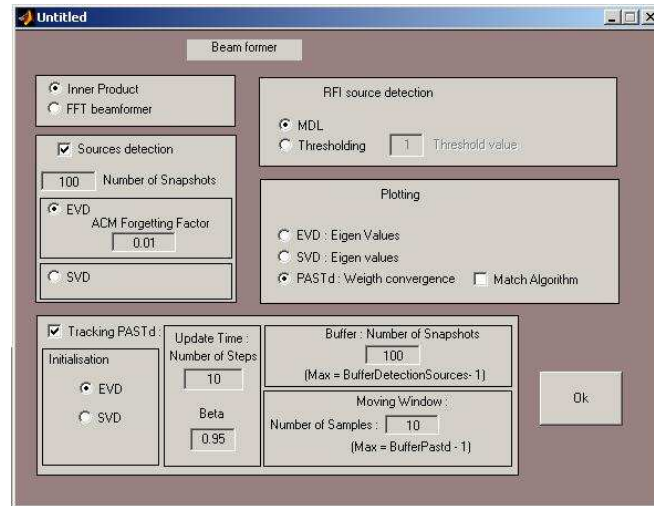


Figure 15: The beamformer configuration window

the Matlab frontend. This allows us to validate the simulation by running the same experiment on both platforms and comparing the results.


Performance of the C++ simulation is indeed much higher than that of its Matlab cousin. It is also capable of running virtually continuously, while the Matlab version is limited by its maximum buffer size in the number of snapshots it can handle. This difference is caused by a fundamental design difference in the two simulations. The Matlab simulation computes the results in a single step using all available snapshots in a large matrix, while the C++ simulation is an event based system which computes results on the way on a snapshot by snapshot basis.

### 4.1.3 Data generators

Data generation was a major issue we identified in the course of this project. Several ad hoc solutions were available both in C++ and in Matlab, but none offered us a representative dataset for our simulation with which we could start experimenting. This prompted the design and implementation of an artificial data generator, which is capable of generating a number of different signals with several different types of modulation and sky sources, both natural as well as man made. The data generator was implemented in Matlab and in C++ in such a way that configuration files generated using the Matlab GUI could seamlessly be integrated in a C++ experiment.[2]

The data generator is capable of producing a signal which can contain one or more separate interfering signals, modulated in a variety of possible ways. Location of the source is calculated for every antenna element in the receiving array. An additional noise floor can be added to simulate natural and system noise.



Author: P.C. Broekema	Date of issue: 2004-May-16 Kind of issue: Limited	Scope: Project documentation Doc.nr.: LOFAR-ASTRON-MEM-136	
	Status: For Review Revision nr.: 1.0	File: <a href="http://dop47.nfra.nl/chris/Thesis/Thesis.pdf">http://dop47.nfra.nl/chris/Thesis/Thesis.pdf</a>	

#### 4.1.4 Limitations of current simulations

The current simulations, both in Matlab as in C++ have several limitations which need to be taken into account when studying any results from them.

The simulators assume perfect receiver units. The antennas are assumed to be omni-directional and noiseless. Since the LOFAR antennas are incapable of movement, this is most definitely an issue for discussion. The LOFAR antenna is of course most sensitive towards the zenith, and least effective near the horizon. Since most interfering sources are assumed to be on the horizon, this can be an advantage. On the other hand, on the northern hemisphere the galactic plane is often only visible near the horizon. Either way, the perfect antenna currently modeled in the software need to be taken into account.


When a source of radiation moves relative to it's observer, we observe a change in frequency. This is known as the *Doppler effect*. The current simulation provides no automated way to add this phenomenon, although the user can do this by hand by calculating the appropriate shift in frequency. Note that the Doppler effect of celestial sources contains components due to it's own movement, as well as components due to the rotation and orbital motion of the earth.

The oscillation of a signal consists of an independent  $x$  and  $y$  component. The relations between these *polarizations* is one of the areas astronomers are most interested in. The current simulation does not take polarization into account. The functionality of the algorithms should not change significantly however, so the fact that we do not currently model this should not be a problem.

The simulator only takes far field signals into account. There is no provision for near field signals. Reflection effects are also not modeled. This could influence the system considerably, so this should be investigated at some later time.

Mutual coupling of the array elements is not modeled at this time. This is a problem that needs to be investigated, but for the purpose of our experiments we have no need for this to be modeled.



Author: P.C. Broekema	Date of issue: 2004-May-16 Kind of issue: Limited	Scope: Project documentation Doc.nr.: LOFAR-ASTRON-MEM-136	
	Status: For Review Revision nr.: 1.0	File: <a href="http://dop47.nfra.nl/chris/Thesis/Thesis.pdf">http://dop47.nfra.nl/chris/Thesis/Thesis.pdf</a>	

## 5 Numerical analysis of the station beamformer

### 5.1 Nulling impact

The LOFAR station may be required to perform some spatial filtering of RFI signals. The beamformer is quite capable of doing this, but any nulling in the beam will have some effects on the beamshape. Goal of this experiment is to measure the effects of a null in the beampattern as a function of the location of the null.

#### 5.1.1 Introduction

Spatial filtering of data at station level is a fundamental part of the LOFAR baseline design. Placing a null in a particular position within the beampattern is a very efficient filtering technique, both in accuracy and in computational cost.


Nulling does introduce distortions in the beamshape. These depend on the position and on the local power of the undisturbed beamshape. Generally we can say that the closer a null is placed to the main lobe, the more powerful the distortion of the beam. Eventually we may need to define a region around the main lobe within which no nulling is allowed. How large this region should be is one of the questions we hope to answer in the following few pages.

#### 5.1.2 Experiment description

For this experiment we use a C++ simulation of a LOFAR station, StationSim. The simulation is configured to point to the zenith while a null is walked slowly from one horizon to the other, crossing the zenith halfway through the experiment. No specific input or output signals are used or measured. We are only interested in the beampattern resulting from the combination of antenna positions, as illustrated earlier in Figure 8, pointing direction and null position.

Placing a null in a beam will have two main effects. First of all the relative power of the main lobe will decrease. This will cause the maximum sidelobe level, as defined in section 5.1.3, to rise. Also, the main lobe will lose some of its narrowness which causes the halfpower beamwidth, also defined in section 5.1.3, to increase. These effects are due to the fact that the total output power of the beamformer is constant, while the distribution of that power is changed.

Figures 16, 17, 18 and 19 illustrate the experiment. These figures show the beamshape as the null is moving over towards the zenith. The effects are, of course, identical on the other side of the zenith due to the symmetric nature of the beam along the line of the null. This is in turn due to the symmetry in the array configuration. These figures are each normalized to it's own maximum, and are therefore not

Author: P.C. Broekema	Date of issue: 2004-May-16 Kind of issue: Limited	Scope: Project documentation Doc.nr.: LOFAR-ASTRON-MEM-136	
	Status: For Review Revision nr.: 1.0	File: <a href="http://dop47.nfra.nl/chris/Thesis/Thesis.pdf">http://dop47.nfra.nl/chris/Thesis/Thesis.pdf</a>	

suitable for any mutual comparison.

### 5.1.3 Quality measures

Two quality measures are used to determine the effects the position of the null has on the beampattern, the maximum sidelobe level (max SLL), and the halfpower beamwidth (HPBW). These measures give an indication of the reduction in power, as well as the distortion of the main lobe.


The maximum sidelobe level is defined as the maximum value outside the main lobe, assuming grating lobes are not an issue. This assumption is in this case valid, since the irregular nature of the chosen array configuration prevents grating lobes from forming. An other configuration of the array should be studied for grating lobes before any conclusions like below can be drawn. Measuring the max SLL is done purely on an algorithmic basis, using the following procedure for a beampattern in dB scale:

1. Find the coordinates for the beam top (the value should be 0 dB here).
2.  $r = 0$
3. Store the maximum of each row in an array  $b$
4. Select a circle  $t$  around the beam top of diameter  $r$
5. All values on the circle are set to  $-\infty$  dB
6. Select the maximum of each row of circle  $t$  in array  $c$
7. if  $(b \neq c)$  {  $x = x+1$ ; goto 3 }
8.  $\text{max-sll} = \max(b)$

The result is, a somewhat rough, estimate of the actual max SLL. The actual resolution of the beampattern used in the experiment is the most obvious reason for this.

The halfpower beamwidth is defined as the maximum width of the beam at -3 dB. Considering the beampattern calculated from the array configuration and the weightvector calculated from the pointing direction and the null position, we select the area of the beampattern with values  $> 3$  dB. The maximum width of the remaining beamtop is determined and returned. This is once again an algorithmic estimation of the actual HPBW.

Both these techniques are estimations of the actual values required. For the purposes of this experiment, this is not an issue. The effects we hope to see should not be affected by these estimates. Analytical methods to determine these measures have been discussed and are in fact used in the next experiment. Time constraints prevented us from repeating the experiment with these methods.

Author: P.C. Broekema	Date of issue: 2004-May-16 Kind of issue: Limited	Scope: Project documentation Doc.nr.: LOFAR-ASTRON-MEM-136	
	Status: For Review Revision nr.: 1.0	File: <a href="http://dop47.nra.nl/chris/Thesis/Thesis.pdf">http://dop47.nra.nl/chris/Thesis/Thesis.pdf</a>	

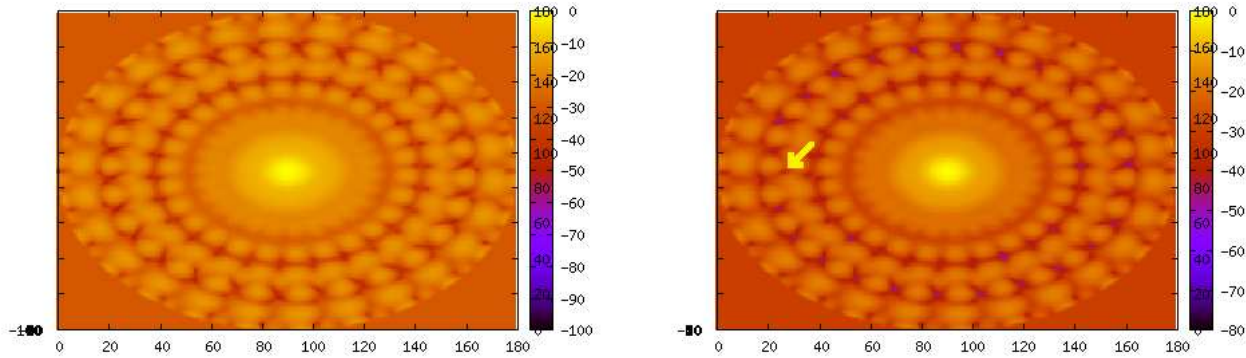


Figure 16: Snapshot 1 and 125. The null can hardly be seen. The yellow arrow points at the null.

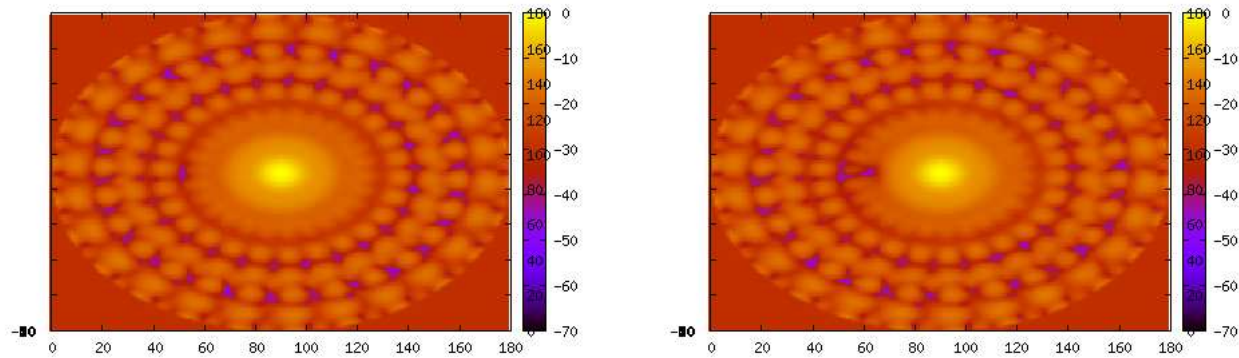



Figure 17: Snapshot 179 and 199. The null is visible, but the beam remains mostly intact.

#### 5.1.4 Experimental results

In five hundred steps, we'll be walking a single null from the left hand side of the beampattern to the right hand side. This trajectory will cross the zenith of the beam (which is, as mentioned before, pointed straight up). We expect the beam to be quite severely distorted when the null approaches the main lobe. Influences outside the main lobe are expected to be apparent, but negligible.

#### 5.1.5 Halfpower beamwidth

Figure 20 shows the halfpower beamwidth set against the position of the null in degrees from the zenith. We can see a stable beam until the null gets within  $7.5^\circ$  of the top. At that point we see first a reduction in halfpower beamwidth. This is caused by a deepening of the first sidelobe around the main lobe, resulting in a narrower beam than normal. Only when placing the null within  $1^\circ$  of the beamtop does the halfpower beamwidth become much larger than normal.

Author: P.C. Broekema	Date of issue: 2004-May-16 Kind of issue: Limited	Scope: Project documentation Doc.nr.: LOFAR-ASTRON-MEM-136	
	Status: For Review Revision nr.: 1.0	File: <a href="http://dop47.nfra.nl/chris/Thesis/Thesis.pdf">http://dop47.nfra.nl/chris/Thesis/Thesis.pdf</a>	

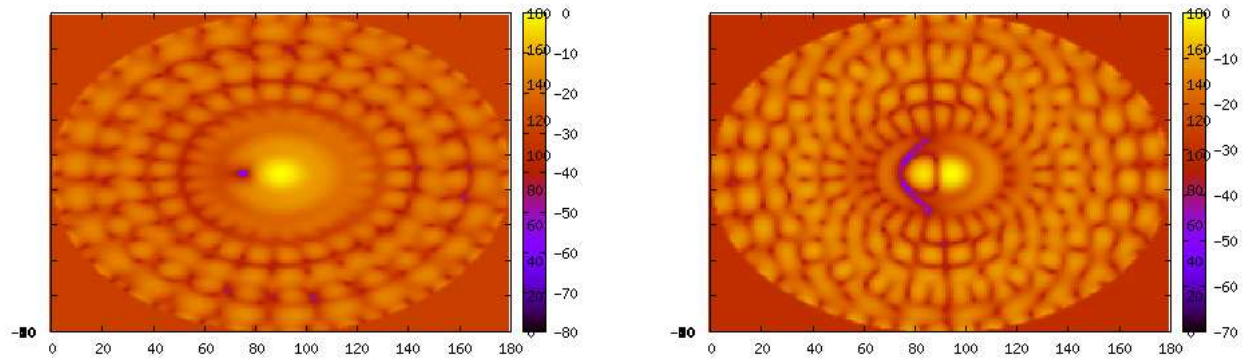


Figure 18: Snapshot 225 and 247. The null enters the main lobe, the beam is severely distorted.

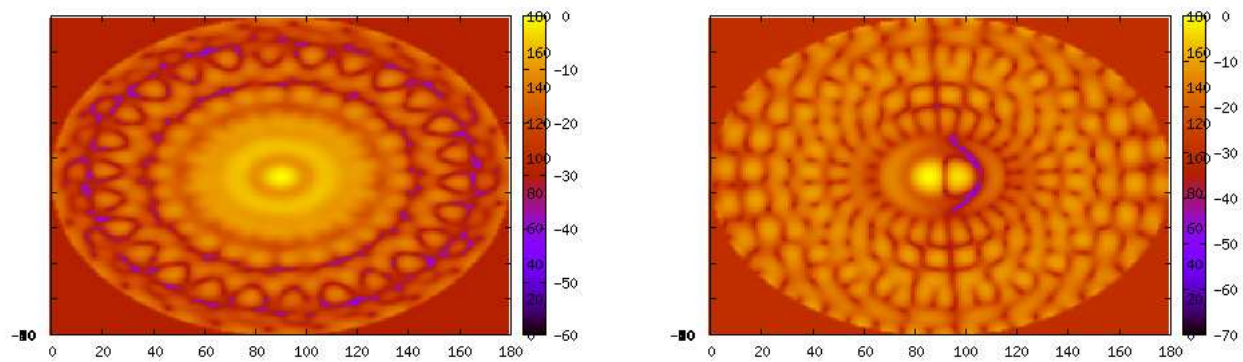



Figure 19: Snapshot 250 and 253. The null in the center of the beam destroys its shape.

Author: P.C. Broekema	Date of issue: 2004-May-16 Kind of issue: Limited	Scope: Project documentation Doc.nr.: LOFAR-ASTRON-MEM-136	
	Status: For Review Revision nr.: 1.0	File: <a href="http://dop47.nfra.nl/chris/Thesis/Thesis.pdf">http://dop47.nfra.nl/chris/Thesis/Thesis.pdf</a>	

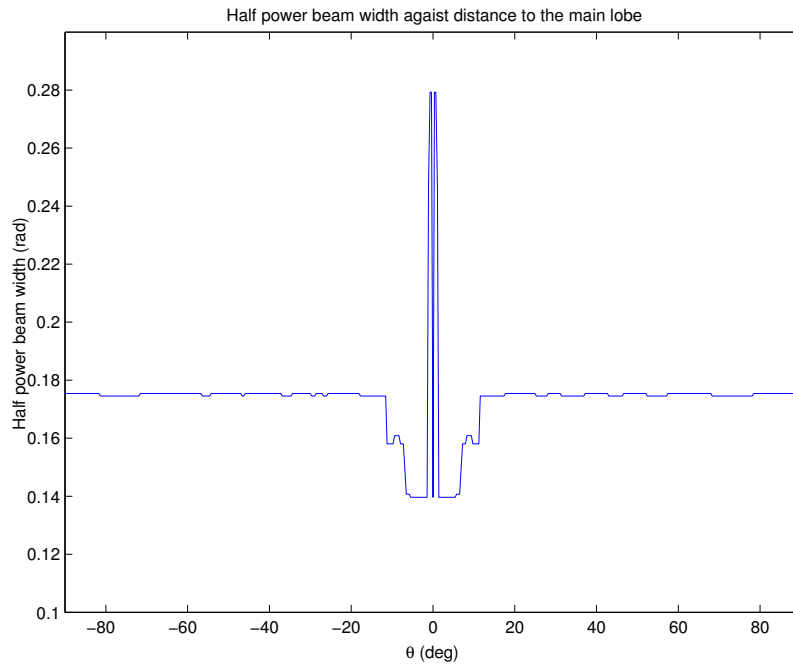



Figure 20: Half power beamwidth against position of the null

In figure 20 we clearly see some discrete jumps in halfpower beamwidth. These jumps are a result of the limited resolution of the experiment and the less than perfect algorithm to calculate the halfpower beam. Also a significant drop in beamwidth is observed when a null is placed at the beamtop. Since the beamwidth is not defined when a null is placed at the top, this is not surprising.

#### 5.1.6 Maximum sidelobe level

Figure 21 shows how the maximum sidelobe level of the beam depends on the direction of the null. The green line shows the actual power of the original beam at the null location, while the blue line represents the maximum sidelobe level with a null at the specified position.

We can once again see that the beam is stable with regards to the maximum sidelobe level, until the null approaches the main lobe within about  $8^\circ$ . Serious rise in sidelobe levels occur when the null gets placed within  $3.2^\circ$  of the beam top. This is caused mainly by the reduction in power of the main lobe in relation to the sidelobes.

Author: P.C. Broekema	Date of issue: 2004-May-16 Kind of issue: Limited	Scope: Project documentation Doc.nr.: LOFAR-ASTRON-MEM-136	
	Status: For Review Revision nr.: 1.0	File: <a href="http://dop47.nfra.nl/chris/Thesis/Thesis.pdf">http://dop47.nfra.nl/chris/Thesis/Thesis.pdf</a>	

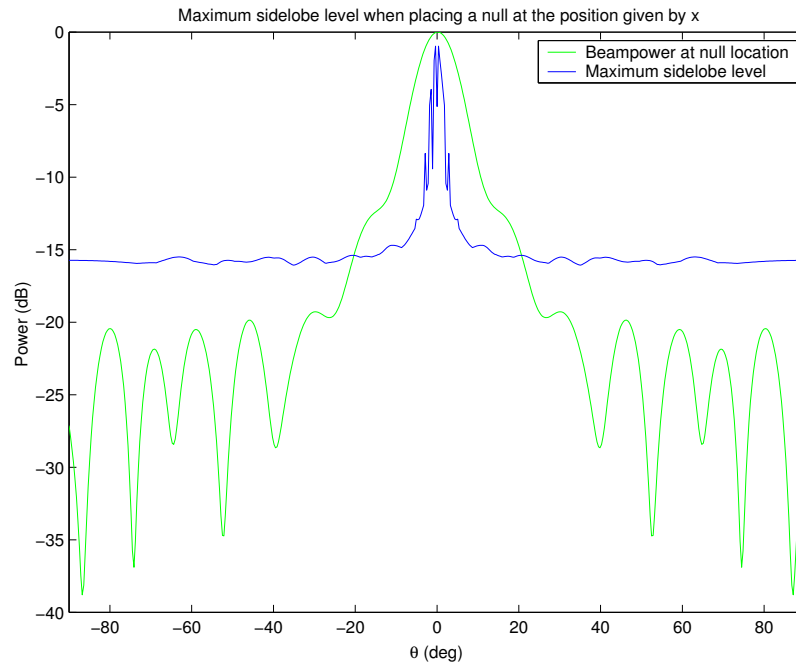


Figure 21: Maximum sidelobe level and actual beampower against position of the null


### 5.1.7 Conclusions and recommendations

This experiment shows that placing a single null in a beam will not influence its shape significantly, unless the null is within  $8^\circ$  of the beam top for this particular array configuration and frequency setting. Even then, the effects don't become pronounced until the null approaches the beam top to within about  $3.2^\circ$ . At first glance we could then conclude that nulls placed at least  $3.2^\circ$  from the beam top could be allowed without significant side effects. Since the array layout in this experiment is measured in  $\lambda$ , the array configuration is independent of frequency. The results of this experiment might change with a different array configuration, but should not depend on frequency.

I would however recommend that all nulls are banned within at least  $8^\circ$  from the beam top. Since we have only studied a single null in this experiment, the addition of more nulls within this area could have significant results. A study into the effects of more nulls on the beamshape would also be wise.

This study concentrated on a single null, a fixed pointing direction and an array configuration which is not certain to be representative of the eventual LOFAR station. The results shown here will depend on any of these factors being changed. Further study into the effects of more nulls, a different array configuration and moving beams is certainly to be recommended. We have shown however that nulling per se, has no ill effects on the beamshape as long as the null stays out of the main lobe.



Author: P.C. Broekema	Date of issue: 2004-May-16 Kind of issue: Limited	Scope: Project documentation Doc.nr.: LOFAR-ASTRON-MEM-136	
	Status: For Review Revision nr.: 1.0	File: <a href="http://dop47.nfra.nl/chris/Thesis/Thesis.pdf">http://dop47.nfra.nl/chris/Thesis/Thesis.pdf</a>	

## 5.2 Beam squint

### 5.2.1 Introduction


In section 2.2.9 we mentioned that the use of complex phase shifters instead of physical time delays in the beamformer introduces a frequency dependent pattern squint. The amount of beamsquint is not yet known, however. All theory concerning this subject assumes regular arrays. The use of irregular array means that the equations are no longer analytically solvable. The following experiment is designed to find a relation between the subband center frequency and the frequency offset. Together with the halfpower beamwidth for these particular frequencies, this will eventually lead to the maximum bandwidth we can safely beamform.

### 5.2.2 Experiment description

To find a measure in which the pattern squint is going to be an issue in the LOFAR remote station beamformer, we need to find the amount of squint as a function to the signal frequency and the subband center frequency. The top of a beam can be described using a second order polynome, as long as the range of the top is chosen small enough. The -3 dB beam of the 92 element array used in the previous experiment is an almost perfect parabola. Since the mathematical properties of second order polynomes are well understood, we will use these properties to our advantage. There are two main parameters to consider in this experiment, the center frequency of the selected frequency band ( $f_c$ ) and the frequency offset we use to calculate the squinted beam ( $\Delta f$ ). The experiment can be summarized as follows:

- Calculate the beampattern for the specified parameters.
- Select the  $-3dB$  beamtop.
- Recalculate the beampattern for this beamtop to achieve higher resolution.
- Discard the sample if the beamtop falls outside the horizon.
- Fit a second order polynome to the zoomed beamtop.
- Determine the top of the polynome
- Compare the top of the polynome to the theoretical beamtop without any squint.
- Determine the halfpower beamwidth of the polynome to get a measure for the relative squint

Calculating the beampattern is done by scanning the sky with a certain resolution, while determining the power of the array in that particular direction. Appendix B shows how this is accomplished.

Author: P.C. Broekema	Date of issue: 2004-May-16 Kind of issue: Limited	Scope: Project documentation Doc.nr.: LOFAR-ASTRON-MEM-136	
	Status: For Review Revision nr.: 1.0	File: <a href="http://dop47.nfra.nl/chris/Thesis/Thesis.pdf">http://dop47.nfra.nl/chris/Thesis/Thesis.pdf</a>	

Since this is quite an intensive algorithm in terms of computational complexity, we calculate the beamtop in two phases. The resolution we achieve this way is far greater than we would even need, with only limited impact on computational load.

Having computed the beamtop, we fit a polynome this top. The second order polynome fitted to the beamtop is of the form:

$$f(x, y) = ax^2 + bxy + cy^2 + dx + ey + f \quad (16)$$

The beamtop is matched to a parabola using a least squares fitting algorithm[3]. The actual algorithm is shown in appendix A.

We expect to find an increasing error in pointing direction with increasing  $\Delta f$ , especially at lower  $f_c$ . Also, the halfpower beamwidth should increase with decreasing frequency.

### 5.2.3 Quality measures

In order to measure the effects that pattern squint has on the beam, we determine the beamtop of the fitted paraboloid. This is done by solving the following set of equations:

$$\frac{\delta f}{\delta x} = 2ax + by + d = 0 \quad \wedge \quad \frac{\delta f}{\delta y} = bx + 2cy + e = 0 \quad (17)$$

Appendix C shows the solution to this set of equations. Having obtained the coordinates of the beamtop, the error is determined compared to the aiming direction at the input. This absolute error should depend on  $\Delta f$  and  $f_c$ .

The beams we use in this experiment are symmetric. This assumption can be made, since the array configuration is symmetric, and we do not place any nulls in the beam. Using this property we can assume that the term  $bxy$  in function 16 is very small, so we can rewrite equation 16 in the form:

$$f(x, y) = a(x - x_0)^2 + c(y - y_0)^2 + f \quad (18)$$

A relatively accurate estimation of the halfpower beamwidth can now be made by determining


$$\max(|x' - x_0|, |y' - y_0|) \quad (19)$$

where  $x'$  and  $y'$  are chosen on the  $-3dB$  contour.

### 5.2.4 Theoretical expectations

Assuming that the lowest frequency presents the greatest challenge with regards to squint, lets see what kind of results we can expect. This will assume a non-sparse and regular array, so eventual results may differ slightly.



Author: P.C. Broekema	Date of issue: 2004-May-16 Kind of issue: Limited	Scope: Project documentation Doc.nr.: LOFAR-ASTRON-MEM-136	
	Status: For Review Revision nr.: 1.0	File: <a href="http://dop47.nrao.nl/chris/Thesis/Thesis.pdf">http://dop47.nrao.nl/chris/Thesis/Thesis.pdf</a>	

The lowest design frequency for LOFAR is about 10 MHz, while the maximum sub-channel bandwidth considered is 256 kHz. In section 2.2.9 we introduced the concept of pattern squint, but we did not quantify this. The amount of beamsquint can be expressed as[11]:

$$a_n = a_0 e^{-\frac{2\pi}{\lambda_0} n d_x u}$$

, where  $u$  is given by:

$$u = u_0 \frac{f_0}{f}$$

This means that for an observed frequency of 10 MHz with a beamformed bandwidth of 256 kHz, a squint factor of  $\frac{10 \cdot 10^6}{10 \cdot 10^6 - 256 \cdot 10^3} \sim 1.03$  is introduced into the beamformer equation. Since this factor weighs heavier as the beam is pointed farther from the zenith, we expect an increasing pattern squint with increasing  $\theta$ . How much this effects the beamformer is not known.

### 5.2.5 Experimental results


First of all, let's look at the resulting beam. Figure 22 shows that the half-power beamwidth of the selected array increases with decreasing frequency. The beamwidth can be estimated using the following rule of thumb:

$$HPBW = \frac{\lambda}{L}, \quad (20)$$

where  $L$  is the largest baseline in the array. The magnitude of this relation depends on the sparseness of the used array. We can visualize this by showing the uv-plane for all possible baselines. Doing so, reveals that only about 80% of the selected array surface is covered. This is illustrated in figure 5.2.5. This is an encouraging result, since it shows that our simulation and our quality measures are working as expected.

The study the actual beamsquint effects, we plot the pointing error ( $\theta_{\text{real}} - \theta_{\text{est}}$ ) against observed frequency  $f$  and pointing direction  $\theta_{\text{real}}$ . The result is figure 23. This figure clearly shows that the beamsquint relates to both observed frequency and looking direction. We can also see that the overall squint effects for the selected 256 kHz bands are quite minor. The major effects seen at looking angles greater than about  $60^\circ$  are an effect of the selected algorithms. Here part of the half-power beam has dropped below the horizon, causing the algorithm to spike.

Since the squint effects are expected to be most pronounced for the lowest frequency, let's take a closer look at the results for the lowest selected frequency, a 1 MHz band around a 15 MHz center frequency. Using the worst case scenario, where the actual frequency is 14 MHz and the center frequency at 15 MHz. We disregard the spike introduced by the half-power beam hitting the horizon and try to extrapolate these values using an exponential function. The results are shown in figure 24. It shows conclusively that the maximum squint for one kHz bands would be around  $15^\circ$ . Looking back at figure 22, we see that the half-power beam at the same frequency is about  $23^\circ$  wide. A 256 kHz band would result in a maximum pattern squint of about  $10^\circ$ .

Author: P.C. Broekema	Date of issue: 2004-May-16 Kind of issue: Limited	Scope: Project documentation Doc.nr.: LOFAR-ASTRON-MEM-136	
	Status: For Review Revision nr.: 1.0	File: <a href="http://dop47.nfra.nl/chris/Thesis/Thesis.pdf">http://dop47.nfra.nl/chris/Thesis/Thesis.pdf</a>	

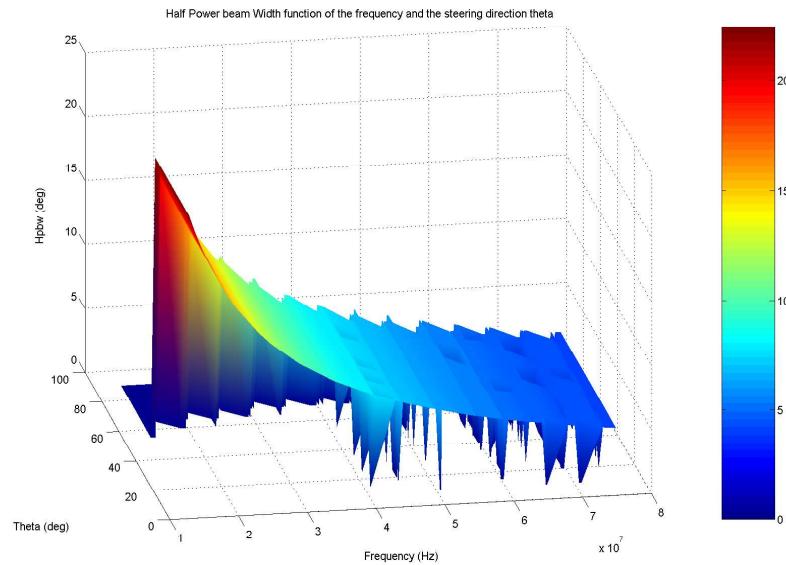


Figure 22: The increasing HPBW against frequency is clearly visible here during the experiment

### 5.2.6 Conclusions and recommendations


This experiment shows that the squint effect is indeed related to bandwidth, frequency and looking direction  $\theta$ . Although the current maximum bandwidth considered for the LOFAR station is 256 kHz, we looked at a wider band of 1 MHz. Even using this wider band, the squint effects are less than the width of the half-power beam. Using a 256 kHz band would at worst result in a pattern squint equal to 0.17 rad, which I would consider quite acceptable. Based on these results I would conclude that using bands of 256 kHz at a center frequency of 15 MHz is, with respect to pattern squint, quite feasible.

## 5.3 Technique evaluation (EVD, SVD, PASTd)

All selected techniques and algorithms were implemented both in Matlab and in C++. Considerable experience was gained in implementing and using these techniques.

We identified a problem using PASTd generated eigen values as an input for MDL. Overall we saw quite unpredictable results when using adaptive beamforming with multiple sources. Especially sources near the main lobe cause the resulting beampattern to be heavily distorted. Although good results can be achieved using adaptive beamforming, we cannot guarantee these results for all interfering sources. The result greatly depends on the location of the source with respect to the main lobe and the sidelobes of the beam.

Estimating the number of interfering sources seems to be unnecessary. Experiments placing far more nulls than interfering sources showed that the eigen value based adaptive beamformer will place lots of

Author: P.C. Broekema	Date of issue: 2004-May-16 Kind of issue: Limited	Scope: Project documentation Doc.nr.: LOFAR-ASTRON-MEM-136	
	Status: For Review Revision nr.: 1.0	File: <a href="http://dop47.nfra.nl/chris/Thesis/Thesis.pdf">http://dop47.nfra.nl/chris/Thesis/Thesis.pdf</a>	

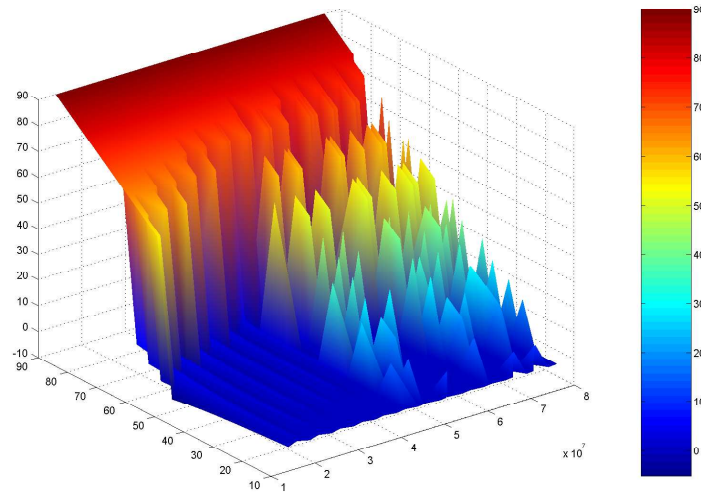


Figure 23: Pointing error due to pattern squint against frequency and pointing direction

nulls around the interfering source. Provided these nulls stay outside the main lobe, the results are better than when placing an exactly calculated number of nulls.

This can be explained by the properties of the placed nulls. We use spatial projection, which causes a very deep, but narrow null. Since interfering sources are almost never point sources, the narrow nulls will never completely cover the interferer. The less significant eigen vectors are in fact vectors pointing at the general area of the interfering source. Placing nulls here helps to completely cover the interferer, improving nulling performance considerably.

We can conclude that, when using an adaptive beamformer based on an Eigen value decomposition technique, we should use more nulls than detected interferers. We have however observed that an increase in the number of placed nulls also increases the distortion of the beam, so there is always a

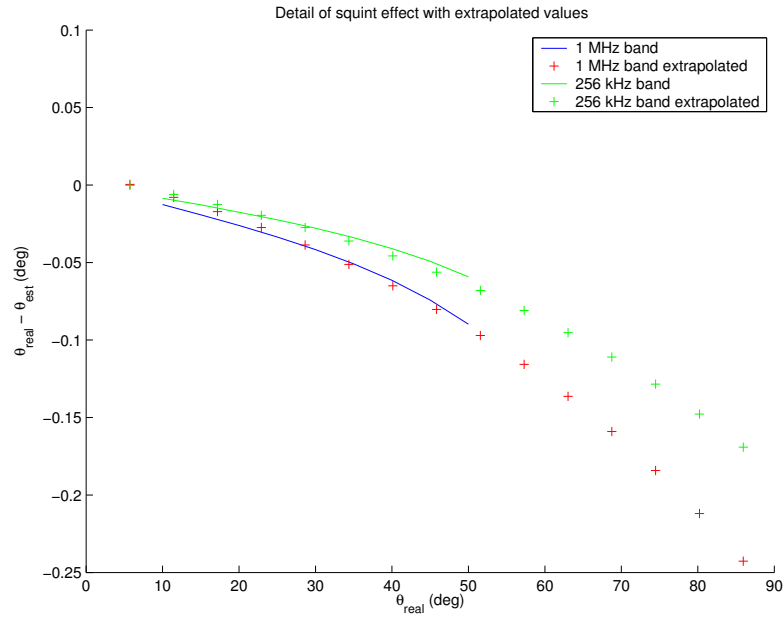


Figure 24: Worst case beamsquint effects using 1 MHz and 256 kHz bands, including extrapolated values

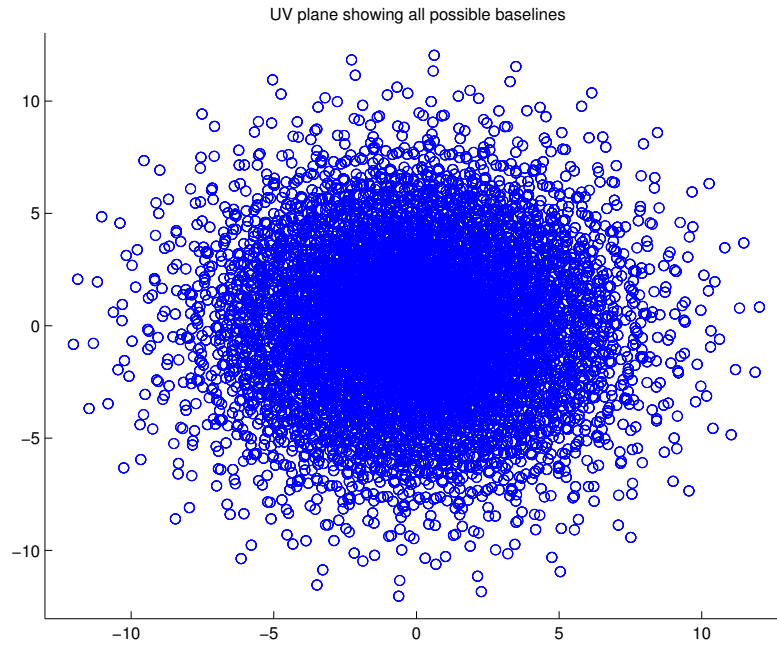



Figure 25: UV plane showing every possible baseline. Note that only about 80% of the area is covered.

Author: P.C. Broekema	Date of issue: 2004-May-16 Kind of issue: Limited	Scope: Project documentation Doc.nr.: LOFAR-ASTRON-MEM-136	
	Status: For Review Revision nr.: 1.0	File: <a href="http://dop47.nfra.nl/chris/Thesis/Thesis.pdf">http://dop47.nfra.nl/chris/Thesis/Thesis.pdf</a>	

## 6 Conclusions and recommendations

A number of conclusions can be drawn from the experiences gained in the course of this project. Unfortunately some of the assumptions made in the beginning are no longer valid.

### 6.1 Baseline design

The baseline design of the station and it's beamformer has changed a bit since the start of this project. The remote station beamformer will still use an inner product beamforming algorithm, and it will be capable of introducing deterministic nulls in the beampattern. Adaptive beamforming will not be included because of the unpredictable nature of these techniques with respect to the resulting beamshape. The advantage of deterministic nulls in this respect is the fact that we can accurately predict the beamshape resulting from an added deterministic null.

Architectural research done by W. Lubberhuizen en M. van Veelen at ASTRON has resulted in the design of a distributed beamforming architecture.[9] This design is illustrated by Figure 26. It basically involves creating a number of beamforming boards connected in a circular pattern. Each board is also connected to it's neighbor to ensure that all antenna signals are added to the beam.

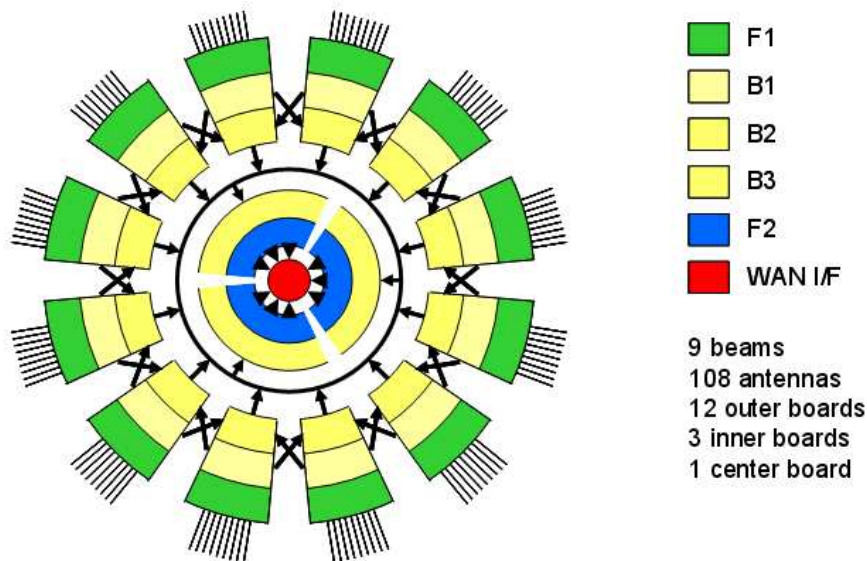



Figure 26: Schematic representation of the distributed beamforming design

Unfortunately the maximum bandwidth we can beamform is still a question that has not been satisfactorily answered. The theory suggests that with some precautions the proposed bandwidth of 256 kHz per subband should be perfectly acceptable, but there is still a need for some numerical or experimental data to confirm this.

Author: P.C. Broekema	Date of issue: 2004-May-16 Kind of issue: Limited	Scope: Project documentation Doc.nr.: LOFAR-ASTRON-MEM-136	
	Status: For Review Revision nr.: 1.0	File: <a href="http://dop47.nfra.nl/chris/Thesis/Thesis.pdf">http://dop47.nfra.nl/chris/Thesis/Thesis.pdf</a>	

## 6.2 Limitations

The results presented here are subject to some limitations. Some of these are of a technical nature, but there are also some limitations to my level of expertise in this area of research.

One of the most significant limitations to the software is the fact that the antenna behavior is mostly unknown at this point, and therefore not modeled in the simulations. All simulations use perfect omnidirectional antennas. Also no polarization of the signal is taken into account. These effects are quite significant and need to be researched. We do not expect the results of this research to be completely opposite of our results, since a perfect omnidirectional antenna is far more sensitive to interfering sources than the LOFAR antennas will be. This is especially true for interfering sources on the horizon, where the LOFAR antenna is the least sensitive, and the RFI occupancy is the highest.

Furthermore, the number of dependencies within the LOFAR remote station beamformer is quite significant. This means that changing a single design parameter can have influences over the entire spectrum of performance measures. Some of the dependencies are shown in figure 27, but this is not an exhaustive list. The dependencies have as a direct consequence that small changes in the design parameters can have large, and sometimes unpredictable consequences on the performance measures. Also, not all dependencies are known, or apparent, making for an even more complicated picture. A single correct answer to our questions on the performance and design of the remote station beamformer is therefore almost impossible to give.

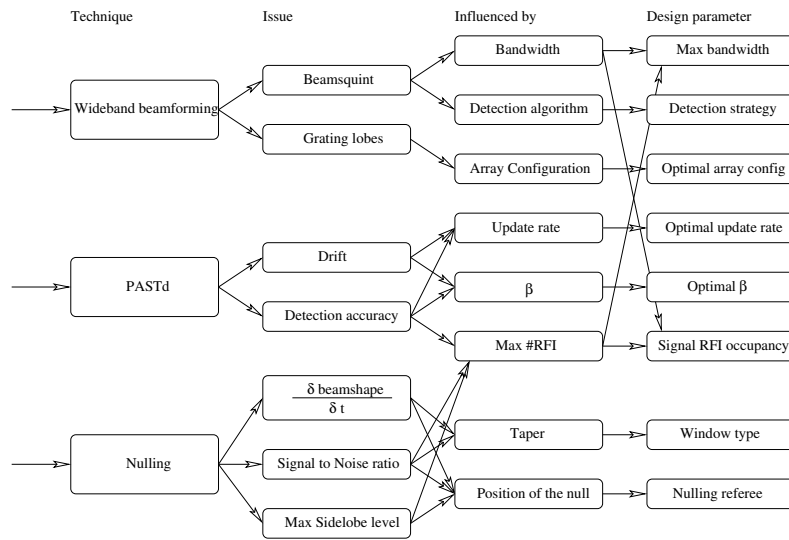



Figure 27: Some dependencies within the LOFAR remote station beamformer

Since the LOFAR project is basically still in the design and feasibility study phase, there is still no real stability of design we could use as a base for our experiments and assumptions. This resulted in, for one thing, the study of adaptive beamforming techniques which proved to be unnecessary. The LOFAR remote station beamformer will now not do any adaptive beamforming and only deterministic

Author: P.C. Broekema	Date of issue: 2004-May-16 Kind of issue: Limited	Scope: Project documentation Doc.nr.: LOFAR-ASTRON-MEM-136	
	Status: For Review Revision nr.: 1.0	File: <a href="http://dop47.nfra.nl/chris/Thesis/Thesis.pdf">http://dop47.nfra.nl/chris/Thesis/Thesis.pdf</a>	

nulls will be allowed in the beams. Reason for this is the fact that adaptive beamforming techniques are, by nature, unpredictable. Since we cannot guarantee the beamformer performance while running an adaptive beamforming algorithm without heavy investment in controlling software development, the adaptive beamforming path was abandoned.

Also the enormous amount of data the LOFAR station is expected to process is very hard to model and simulate. We can easily create a simulator for the algorithms under study, but we can never hope to reach the datarates eventually needed for the LOFAR station. This means that we are bound to run into problems later on in the project related to the high datarates involved.


### 6.3 Recommendations

Further research on the LOFAR station and more particular the LOFAR remote station beamformer should from this point on concentrate on real measurements wherever possible. The first batch of hardware is available in prototype form for these purposes and we have seen that simulating has it's share of disadvantages over real data.

Calibration and filter design are two vital parts of the LOFAR remote station development that are outside the scope of this thesis.

As a final recommendation I would stress that, on the whole, the ancient wisdom of KISS (Keep It Simple, Stupid) still applies. The LOFAR project is, frankly, huge. In order to be able to control performance from one end of the spectrum (for instance antenna performance) to the other (say, the end result of a measurement stretching over a period of twelve hours) all blocks need to be designed with clear performance guarantees. Without these, the end result can never be estimated with total security. Strict guidelines are therefore a must, and the simplest way to abide by them is to use simple and well understood algorithms.



Author: P.C. Broekema	Date of issue: 2004-May-16 Kind of issue: Limited	Scope: Project documentation Doc.nr.: LOFAR-ASTRON-MEM-136	
	Status: For Review Revision nr.: 1.0	File: <a href="http://dop47.nfra.nl/chris/Thesis/Thesis.pdf">http://dop47.nfra.nl/chris/Thesis/Thesis.pdf</a>	

## 7 Final words

### 7.1 Personal review

Unfortunately I cannot call my masters project a complete success. When starting this project I assumed I could give a complete and clear answer to all questions regarding the remote station beamformer. This proved to be impossible. The reasons for this are diverse, and most are mentioned in the previous chapter. I do want to place some self criticism in this section.

I have spent far to much time on implementation and debugging of the C++ simulation. It was planned from the beginning to make the Matlab simulation work, and later port it to C++ to provide a faster simulation platform. Looking back on this project I realize that this was not a good idea, and my efforts should have been concentrated on the Matlab simulations. This may have enabled me to do more, albeit slower experiments than are currently presented in this thesis.

The fact that the remote station simulation is available right now does provide the experience needed to further develop the LOFAR station software that is being developed right now, so the time spent on the development of the simulation was not wasted.


Also I have concentrated too much effort on the analysis of the adaptive algorithms of the beamformer. When it was decided not to do any adaptive beamforming on the remote station, this work became less important which was a bit of a disappointment to me.

### 7.2 Acknowledgments

I would like to mention some persons without whom this thesis would not have been possible. In no particular order these persons are:


- Sylvain Alliot - Sylvain basically handed me the basics of the station beamformer on a platter. He was instrumental in the first couple of weeks of my time at ASTRON, helping me along on the theoretical plane while explaining some of his software at other times.
- Jerome Dromer - Jerome was especially helpful in the later stages of this project. His expertise in signal processing was especially welcome. Also, he created a signal generator design which enabled us to create relatively realistic signals for the station simulations. He also worked extensively on the Matlab simulation and provided a lot of feedback during the reviews of this document which were improved the quality of the document a lot.
- Alex Gerdes - Alex worked tirelessly along side me building and later debugging StationSim. Together we generated a complex piece of software capable of simulating an entire LOFAR remote station. His work on the data generator and polyphase filterbank as well as the top level simulator



Author: P.C. Broekema	Date of issue: 2004-May-16 Kind of issue: Limited	Scope: Project documentation Doc.nr.: LOFAR-ASTRON-MEM-136	
	Status: For Review Revision nr.: 1.0	File: <a href="http://dop47.nfra.nl/chris/Thesis/Thesis.pdf">http://dop47.nfra.nl/chris/Thesis/Thesis.pdf</a>	


was extensive. He also was able to improve the overall performance of the simulation by an impressive factor. Results from this new simulation have not been included in this thesis, unfortunately.

- Stefan Wijnholds - Stefan was instrumental in the final stages of this project. His theoretical insight provided the basis for the analytical way in which the beamsquint experiment was performed. He also proved invaluable input as a reviewer, picking up even the most obscure spelling mistake and providing clear and well founded feedback on the entire document.
- Martijn van Veelen - My supervisor at ASTRON, he offered advise and support even when I didn't think I needed it. He was right, of course. He also had enough confidence in me to arrange a job offer at ASTRON for me, which I gratefully accepted. Added to that was the carpool arrangement we made for the duration of my thesis period.


Author: P.C. Broekema	Date of issue: 2004-May-16 Kind of issue: Limited	Scope: Project documentation Doc.nr.: LOFAR-ASTRON-MEM-136	
	Status: For Review Revision nr.: 1.0	File: <a href="http://dop47.nfra.nl/chris/Thesis/Thesis.pdf">http://dop47.nfra.nl/chris/Thesis/Thesis.pdf</a>	

## References

- [1] S. Alliot. Station digital processing architectural design document (lofar-astron-add-007). Technical report, ASTRON - the LOFAR project, October 2002.
- [2] J. Dromer, P.C. Broekema, and M. van Veelen. Data generators design and implementation. Technical report, ASTRON - the LOFAR project, November 2003.
- [3] David Eberly. Least squares fitting of data. <http://www.magic-software.com>, July 1999.
- [4] Steven W. Ellingson and G.A. Hampson. A subspace-tracking approach to interference nulling for phased array-based radio telescopes. *IEEE transactions on Antennas and propagation*, 50:25–30, January 2002.
- [5] Malcolm Goris, Antony Joseph, Grant Hampson, and Felix Smits. An adaptive beamforming system for radio-frequency interference rejection. In *IEE proceedings Radar, Sonar and Navigation*, volume 146, pages 73–77, April 1999.
- [6] Johan Hamaker. Instrumental techniques of aperture synthesis, spring 1997.
- [7] G. Hampson and W. Cazemier. THEA project (SKA), the development of a single dimension adaptive interference suppression algorithm. Technical report, Astron, 2000.
- [8] R.C. Hansen. *Phased Array Antennas*. Wiley series in microwave and optical engineering. John Wiley & Sons, Inc., 1998.
- [9] W. Lubberhuizen and M. van Veelen. An architecture with distributed beamforming (lofar-astron-mem-082). Technical report, ASTRON - the LOFAR project, May 2003.
- [10] V.K. Madisetti and D.B. Williams, editors. *the Digital Signal Processing Handbook*. CRC Press, 1998.
- [11] Robert J. Mailloux. *Phased Array Antenna Handbook*. Artech house, 1993.
- [12] W.P. Press et al. *Numerical recipes in C*. Cambridge University Press, second edition edition, 1992.
- [13] F. Stokkel and M. van Veelen. Station digital processing subsystem requirement specification (lofar-astron-srs-003). Technical report, ASTRON - the LOFAR project, October 2002.
- [14] G.B. Taylor, C.L. Carilli, and R.A. Perley, editors. *Synthesis imaging in radio astronomy II*. Astronomical Society of the Pacific, 1999.
- [15] M. van Veelen. Pre-correlation algorithm theoretical basis document (lofar-astron-doc-006). Technical report, ASTRON - the LOFAR project, 2002.
- [16] Stefan J. Wijnholds. Pre-correlation signal processing baseline (lofar-astron-mem-105). Technical report, ASTRON - the LOFAR Project, November 2003.

Author: P.C. Broekema	Date of issue: 2004-May-16 Kind of issue: Limited	Scope: Project documentation Doc.nr.: LOFAR-ASTRON-MEM-136	
	Status: For Review Revision nr.: 1.0	File: <a href="http://dop47.nfra.nl/chris/Thesis/Thesis.pdf">http://dop47.nfra.nl/chris/Thesis/Thesis.pdf</a>	

- [17] Stefan J. Wijnholds. Station calibration approach (lofar-astron-mem-093). Technical report, ASTRON - the LOFAR project, 2003.
- [18] Bin Yang. Projection approximation subspace tracking. In *IEEE Transactions on signal processing*, volume 43, pages 95–107, January 1995.

Author: P.C. Broekema	Date of issue: 2004-May-16 Kind of issue: Limited	Scope: Project documentation Doc.nr.: LOFAR-ASTRON-MEM-136	
	Status: For Review Revision nr.: 1.0	File: <a href="http://dop47.nfra.nl/chris/Thesis/Thesis.pdf">http://dop47.nfra.nl/chris/Thesis/Thesis.pdf</a>	

## A Fitting of a second order paraboloid

```
%
% This function is based on a C++ implementation by Magic Software Inc.
% http://www.magic-software.com
%

%
% Matlab implementation (C) 2003 Astron (Netherlands Foundation for Research in Astronomy)
% by Chris Broekema, july 2003
%

% Fitting a paraboloid unsing least squares
%
% Given a set of samples (akPoints_x(i), akPoints_y(i), akPoints_z(i)) for 1 <= i <= N
% and assuming that the true values lie on a paraboloid
%  $x = p0*x*x + p1*x*y + p2*y*y + p3*x + p4*y + p5 = \text{Dot}(P, Q(x,y))$ 

function [resCoeff] = paraboloidFit (nrPoints, akPoints_x, akPoints_y, akPoints_z)

% allocate linear system (A and b are zeroed)
A = zeros(6,6);
afCoeff = zeros(1,6);

for (i=1:nrPoints)
    A(1, 1) = A(1, 1) + akPoints_x(i)^4;
    A(1, 2) = A(1, 2) + akPoints_x(i)^3 * akPoints_y(i);
    A(1, 3) = A(1, 3) + akPoints_x(i)^2 * akPoints_y(i)^2;
    A(1, 4) = A(1, 4) + akPoints_x(i)^3;
    A(1, 5) = A(1, 5) + akPoints_x(i)^2 * akPoints_y(i);
    A(1, 6) = A(1, 6) + akPoints_x(i)^2;

    A(2, 3) = A(2, 3) + akPoints_x(i) * akPoints_y(i)^3;
    A(2, 5) = A(2, 5) + akPoints_x(i) * akPoints_y(i)^2;
    A(2, 6) = A(2, 6) + akPoints_x(i) * akPoints_y(i);


    A(3, 3) = A(3, 3) + akPoints_y(i)^4;
    A(3, 5) = A(3, 5) + akPoints_y(i)^3;
    A(3, 6) = A(3, 6) + akPoints_y(i)^2;

    A(4, 4) = A(4, 4) + akPoints_x(i)^2;
    A(4, 6) = A(4, 6) + akPoints_x(i);

    A(5, 6) = A(5, 6) + akPoints_y(i);

    afCoeff(1) = afCoeff(1) + akPoints_z(i) * akPoints_x(i)^2;
    afCoeff(2) = afCoeff(2) + akPoints_z(i) * akPoints_x(i) * akPoints_y(i);
    afCoeff(3) = afCoeff(3) + akPoints_z(i) * akPoints_y(i)^2;
    afCoeff(4) = afCoeff(4) + akPoints_z(i) * akPoints_x(i);
    afCoeff(5) = afCoeff(5) + akPoints_z(i) * akPoints_y(i);
    afCoeff(6) = afCoeff(6) + akPoints_z(i);
end

A(2, 1) = A(1, 2);
A(2, 2) = A(1, 3);
A(2, 4) = A(1, 5);
A(3, 1) = A(1, 3);
A(3, 2) = A(2, 3);
A(3, 4) = A(2, 5);
```

Author: P.C. Broekema	Date of issue: 2004-May-16 Kind of issue: Limited	Scope: Project documentation Doc.nr.: LOFAR-ASTRON-MEM-136	
	Status: For Review Revision nr.: 1.0	File: <a href="http://dop47.nfra.nl/chris/Thesis/Thesis.pdf">http://dop47.nfra.nl/chris/Thesis/Thesis.pdf</a>	


```

A(4, 1) = A(1, 4);
A(4, 2) = A(2, 4);
A(4, 3) = A(3, 4);
A(4, 5) = A(2, 6);
A(5, 1) = A(1, 5);
A(5, 2) = A(2, 5);
A(5, 3) = A(3, 5);
A(5, 4) = A(4, 5);
A(5, 5) = A(3, 6);
A(6, 1) = A(1, 6);
A(6, 2) = A(2, 6);
A(6, 3) = A(3, 6);
A(6, 4) = A(4, 6);
A(6, 5) = A(5, 6);
A(6, 6) = nrPoints;

```

```
% The system of linear equations is now defined.
```


```
resCoeff = A\afCoeff.');
```

Author: P.C. Broekema	Date of issue: 2004-May-16 Kind of issue: Limited	Scope: Project documentation Doc.nr.: LOFAR-ASTRON-MEM-136	
	Status: For Review Revision nr.: 1.0	File: <a href="http://dop47.nfra.nl/chris/Thesis/Thesis.pdf">http://dop47.nfra.nl/chris/Thesis/Thesis.pdf</a>	

## B Scanning the sky

```
function a = steerv(px, py, phi, theta, LAMDA)
a = exp(i*2*pi/LAMBDA*(px*sin(theta)*cos(phi)+py*sin(theta)*sin(phi)));

function pattern = generate_beam (px, py, phi_steer, theta_steer, N,LAMBDA)
WeightVector = steerv(px, py, phi_steer, theta_steer, LAMBDA); // steer the beam
for idx_u = 1:dimu
    for idx_v = 1:dimv
        if (sqrt(u(idx_u)^2 + v(idx_v)^2) < 1);
            pat(idx_u, idx_v) = exp(-2 * pi * sqrt(-1) * (px * (v(idx_v) ) + py * (u(idx_u) )) / LAMBDA)*WeightVector;
        else
            pat(idx_u, idx_v)=0; // below the horizon
        end
    end
end
end
pattern = abs(pat)/max(max(abs(pat)));
```

Author: P.C. Broekema	Date of issue: 2004-May-16 Kind of issue: Limited	Scope: Project documentation Doc.nr.: LOFAR-ASTRON-MEM-136	
	Status: For Review Revision nr.: 1.0	File: <a href="http://dop47.nfra.nl/chris/Thesis/Thesis.pdf">http://dop47.nfra.nl/chris/Thesis/Thesis.pdf</a>	

## C Solving a set of equations

$$\begin{aligned}
 f(x, y) &= ax^2 + bxy + cy^2 + dx + ey + f \\
 \frac{\delta f}{\delta x} &= 2ax + by + d = 0 \\
 \Leftrightarrow by &= -2ax - d \\
 \Leftrightarrow y &= -\frac{2a}{b}x - \frac{d}{b}
 \end{aligned} \tag{21}$$

$$\begin{aligned}
 \frac{\delta f}{\delta y} &= bx + 2cy + e = 0 \quad \wedge \quad y = -\frac{2a}{b}x - \frac{d}{b} \\
 \Leftrightarrow 2c \left( -\frac{2a}{b}x - \frac{d}{b} \right) &+ bx + e = 0 \\
 \Leftrightarrow -\frac{4ac}{b}x - \frac{2cd}{b} &+ bx + e = 0 \\
 \Leftrightarrow \left( b - \frac{4ac}{b} \right) x &= \frac{2cd}{b} - e \\
 \Leftrightarrow x &= \frac{\frac{2cd}{b} - e}{b - \frac{4ac}{b}} \\
 \Leftrightarrow x &= \frac{\frac{2cd - eb}{b}}{\frac{b^2 - 4ac}{b}} \\
 \Leftrightarrow x &= \frac{2cd - eb}{b} \cdot \frac{b}{b^2 - 4ac} \\
 \Leftrightarrow x &= \frac{2cd - eb}{b^2 - 4ac}
 \end{aligned} \tag{22}$$

$$\begin{aligned}
 y &= -\frac{2a}{b}x - \frac{d}{b} \quad \wedge \quad x = \frac{2cd - eb}{b^2 - 4ac} \\
 \Leftrightarrow y &= -\frac{2a}{b} \cdot \frac{2cd - eb}{b^2 - 4ac} - \frac{d}{b} \\
 \Leftrightarrow y &= \frac{-2a(2cd - eb) - d(b^2 - 4ac)}{b(b^2 - 4ac)} \\
 \Leftrightarrow y &= \frac{2abe - db^2}{b(b^2 - 4ac)} \\
 \Leftrightarrow y &= \frac{2ae - db}{b^2 - 4ac}
 \end{aligned} \tag{23}$$